Multiscale and Multidisciplinary Modeling, Experiments and Design (2025) 8:287
https://doi.org/10.1007/s41939-025-00873-5

ORIGINAL PAPER

Analysis of the influence of cutting parameters on AISI M32C high-speed steel tool temperature using inverse heat conduction techniques

Rogério Fernandes Brito[1] · Ricardo Luiz Perez Teixeira[1] · Heitor Alves Falqueto[1] · Giovani Wilhan Viana Carvalho[1] · José Carlos de Lacerda[1] · Tarcísio Gonçalves de Brito[1] · Paulo Mohallem Guimarães[1] · Sandro Metrevelle Marcondes de Lima e Silva[1] · Solidônio Rodrigues de Carvalho[2] · Júlio Cesar Costa Campos[3]

Received: 24 January 2025 / Accepted: 16 April 2025

Abstract
The effect of cutting parameters—workpiece rotation speed, depth of cut, and feed rate—on the temperature distribution across the rake face of an AISI M32C high-speed steel cutting tool is analyzed. The study focuses on machining ABNT 12L14 steel to evaluate thermal behavior under different cutting conditions. Using COMSOL® Multiphysics 6.0 for 3D transient heat transfer modeling, three inverse methods-Levenberg–Marquardt, Linear Specified Function, and Nelder-Mead-to estimate heat flux at the chip-tool interface are implemented. Our results show that the Levenberg–Marquardt method achieves the best accuracy, with estimated temperatures deviating by only 1.5% from experimental measurements. This study highlights the effectiveness of optimized cutting parameters in minimizing tool temperature and extending tool life, with the proposed method offering practical benefits for industrial machining processes.

Keywords Heat transfer · Inverse methods · Levenberg–Marquardt · Linear specified function · Machining · Nelder-Mead

1 Introduction

Temperature control is a critical factor in machining processes, directly influencing tool performance, wear resistance, and the quality of the machined surface. Excessive heat generated at the chip-tool interface can lead to accelerated tool degradation, impacting productivity and efficiency while incurring additional costs. Accurate temperature estimation and effective heat management are essential for optimizing machining processes and extending tool life (Trent et al. 2025; Brito et al. 2015; Kovac et al. 2019). This study investigates the influence of cutting parameters on tool temperature and employs inverse heat conduction techniques to obtain precise temperature estimates at the tool-workpiece interface.

1.1 Temperature measurement and inverse problems in machining processes

Temperature measurement during machining is challenging due to the dynamic and localized nature of the heat generated at the chip-tool interface (Brito et al. 2009; Paula et al. 2019; Diniz et al. 2005; D'Addona and Raykar 2019). Previous studies have employed techniques such as thermocouples and infrared cameras to capture temperature profiles, but these methods face limitations in obtaining direct measurements at exact contact points, resulting in potential inaccuracies (Brito et al. 2015; Diniz et al. 2005). Inverse problems have increasingly been utilized to overcome these limitations, indirectly estimating temperature and heat flux at the interface based on accessible measurements from nearby points. This method has shown promise in enhancing the accuracy of temperature

✉ Ricardo Luiz Perez Teixeira
ricardo.luiz@unifei.edu.br

[1] Federal University of Itajubá, UNIFEI, Campus Prof. Jose Rodrigues Seabra, Avenida BPS 1303, Itajubá, MG 37500-903, Brazil

[2] College of Mechanical Engineering, Federal University of Uberlandia, UFU, Campus Santa Monica, Bloco M, Avenida Joao Naves dé Avila 2121, Uberlândia, MG 38408-100, Brazil

[3] Department of Production and Mechanical Engineering - DEP, Laboratory of Thermal Systems - LST, Federal University of Viçosa - UFV, Viçosa, MG 36570-900, Brazil

Published online: 02 May 2025

predictions in machining processes (Machado et al. 2015; Lima et al. 2000; Carvalho et al. 2006). Additional work is needed to refine these models, particularly in accounting for transient cutting conditions, though.

This study is based on the numerical and experimental work of Santos et al. (2014). They demonstrated that, within the tested range of heat transfer coefficients by convection (h) of 10–30 W/m^2·K, the influence on the final temperature at the cutting interface was minimal. Using an average h value of 20 W/m^2·K as a reference, a maximum deviation of less than 0.74% was observed in the calculated temperature compared to other h values within the range. From these results (Santos et al. 2014), it was concluded that temperature calculations at the cutting interface were reliable and did not compromise for the h values considered, leading to the adoption of 20 W/m^2·K as a standard reference value. The temperature range, over which the material properties were considered, was clearly defined. The computational simulation incorporated temperature dependent thermophysical properties of the cutting apparatus. This ensured accurate thermal analysis. Specifically, the initial temperature throughout the computational domain was set to 0 °C during sensitivity coefficient calculations. The experimental and numerical analyses covered a range where maximum tool temperatures reached 570 °C and minimum tool temperatures did not exceed 160 °C (Santos et al. 2014). These values were used to validate the numerical model and optimize heat flux estimation techniques in order to ensure consistency in the material properties applied across different cutting conditions.

1.2 Experimental methods for obtaining temperature at the cutting interface

Direct temperature measurement methods, such as embedded thermocouples, infrared cameras, and thin-film thermocouples (TFTCs), have been widely used to obtain temperature data in machining studies. While these methods provide valuable insights into heat generation and tool wear, challenges persist regarding sensor placement and response time, which can introduce discrepancies in measurements (Kshetri et al. 2020; Chen et al. 2017; Soler et al. 2018). The thermocouples used are the K-type Thermocouple, which introduces a deviation of about ± 2 °C for the range of temperature present. For instance, Chen et al. (2017) used thermocouples to measure the temperature on the wear surface of cutting tools. Soler et al. (2018) employed an infrared thermal camera for greater precision. De-spite advancements, these experimental techniques are often limited by environmental constraints, emphasizing the need for a complementary approach that integrates both experimental data and numerical modeling.

1.3 Analytical, numerical, and inverse techniques for solving the machining thermal problem

Addressing thermal challenges in machining requires a combination of analytical, numerical, and inverse techniques to accurately predict temperature distribution. Analytical models are effective for simpler systems. However, they may exhibit deviations due to necessary simplifications (Kashani et al. 2016). Numerical techniques, such as Finite Element Analysis (FEA), enable more detailed simulations and suit complex geometries that are typical from machining. Nevertheless, these methods have a high computational cost (Clavier et al. 2021; Kanellos et al. 2019). Inverse techniques, such as the Levenberg–Marquardt, Linear Specified Function, and Nelder-Mead methods, have been employed to estimate thermal properties more accurately, resolving heat flux issues on the cutting tool surface (Dourado da Silva et al. 2021). This study applies these inverse techniques in COMSOL® Multiphysics to enhance the precision of temperature estimations by providing a practical solution to optimize cutting conditions in machining processes (Heat 2018).

COMSOL® Multiphysics employs Finite Element Analysis (FEA), even though Finite Difference Method (FDM) is more computationally efficient for simple geometries and uniform grids. However, FEA proves to be more effective in handling complex geometries and adaptive meshes, where the grid can be refined in regions of interest (Thornton and Wieting 1979). FEA also offers greater flexibility in managing complex boundary conditions, such as non-uniform heat flux or convective boundaries, by directly incorporating these conditions into the element equations (Thornton and Wieting 1979).

The numerical simulations were conducted using the commercial software COMSOL® Multiphysics 5.6 (Heat 2018). In the COMSOL® interface, the transient heat transfer in the solid module was employed to address the physics of the problem. Once this module is selected, the software provides standard numerical methods for solving the physical model. This feature is a major advantage of the software, that is, selecting a specific module for a given physics automatically defines numerical methods optimized for achieving better convergence with minimal computational time.

For transient heat transfer problems, COMSOL® Multiphysics utilizes the second-order Backward Differentiation Formula (BDF) method to approximate time derivatives. BDF is an implicit multi-step numerical integration method used for solving ordinary differential equations (Heat 2018). In a BDF of order n, the problem is solved using a polynomial of degree n, incorporating terms derived from previous steps.

To solve the linear system of equations generated by the Finite Element Method (FEM), the heat transfer module in

COMSOL® Multiphysics applies the Parallel Sparse Direct and Multi-Recursive Iterative Linear Solvers (PARDISO) method for a small number of degrees of freedom. The PARDISO method is a high-performance and robust approach for solving symmetric or non-symmetric sparse linear systems in the form $Ax = b$ (PARDISO-PROJECT 2019).

1.4 Research gaps and objectives

Despite the advances made in measuring and modeling thermal behavior in machining, precise temperature estimation at the chip-tool interface remains a challenge. This study addresses this gap by using inverse heat conduction techniques to achieve accurate temperature distribution predictions, focusing on optimizing cutting parameters to minimize tool temperature. By analyzing workpiece rotation speed, depth of cut, and feed rate, this research aims to provide valuable insights that support improved tool life and process efficiency, offering a refined approach to thermal management in machining.

2 Methodology

This machining process, conducted by Santos et al. (2014), utilized a Revolution RV220 Diplomat lathe and a workpiece, which is made of free-machining steel AISI 12L14. The workpiece had a diameter of 50.8 mm and underwent a hot-rolled treatment, resulting in a Rockwell B hardness of 68 and a ferritic microstructure. These material properties and machining conditions were critical for analyzing tool performance and thermal behavior during the cutting process.

The validation of techniques used in solving inverse heat conduction problems presents a significant challenge. This difficulty arises because validating the estimated heat flux requires prior knowledge of the experimental heat flux. In real-world inverse problems, such as those encountered in machining processes, the experimental heat flux is often unknown. To address this, an alternative validation approach involves conducting controlled experiments. In such experiments, heat flux and temperature measurements are taken from the cutting tool. These measured signals are compared with the estimated heat flux. Hence, temperatures are calculated using the COMSOL Multiphysics software for three inverse techniques. Prior to analyzing the real machining process, a controlled experiment was performed using a cemented carbide tool with dimensions of 0.0127 m × 0.0127 m × 0.0047 m, as explained by Carvalho et al. (2006). The authors employed a setup that included a heat flux transducer, two previously calibrated thermocouples, and a Kapton electric heater, as shown in Fig. 1.

As an experimental strategy, the study utilized the experimental data from Carvalho et al. (2006), by employing the

Fig. 1 Kapton electric heater. Source: TEMPCO (2025)

experimental setup, shown in Fig. 2. In this case, the results obtained through COMSOL® simulations were compared with the referenced data to validate the mathematical modeling used in the present study.

In the experimental setup, the electric heater connected to a continuous source current (MCE), generated heat through the Joule effect. The heat flux transducer was positioned between the heater and the tool to measure the heat supplied, as depicted in Fig. 2. Temperature readings were obtained using the two thermocouples. Data acquisition involved an HP Series 75,000 system with the E1326B voltmeter controlled by a PC. To ensure optimal thermal contact, thermal paste was applied between the transducer and the tool. Capacitor discharge facilitated the attachment of the thermocouples to the plate surface.

The present study developed a numerical methodology for the validation of direct and inverse problems using a cemented carbide cutting tool, as previously investigated by Carvalho et al. (2006). For the direct problem, numerical temperature estimates were obtained using the Finite Element Methodology (FEM) using COMSOL Multiphysics software (Heat 2018).

The estimated heat fluxes in the cemented carbide cutting tool were obtained using inverse techniques, utilizing the experimental temperatures from Carvalho et al. (2006). The comparative analysis employed three inverse techniques: Nelder-Mead (NM), Levenberg–Marquardt (LM), and Linearly Specified Function (LSF). After conducting the experiment, validation was performed for both the direct and inverse problems in the present study. It was observed that the Levenberg–Marquardt (LM) technique achieved a better computational cost ratio.

The inverse problem was solved and applied to cases of easy-cutting steel turning with high-speed steel tools for varied cutting tool parameters. Each technique has its advantages and disadvantages, and the choice depends on the specific

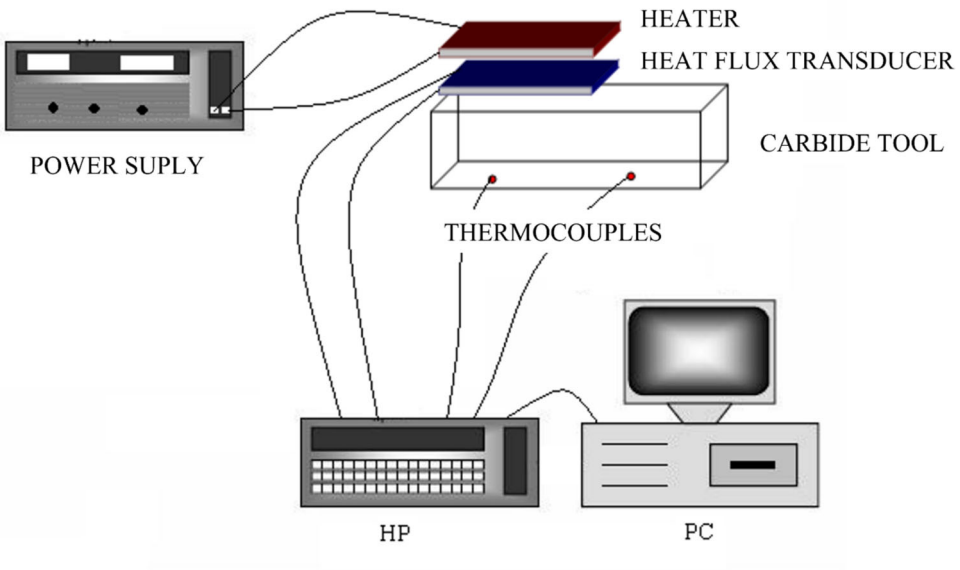

Fig. 2 Schematic of the experimental set-up made by Carvalho et al. (2006). Source: Santos (2008)

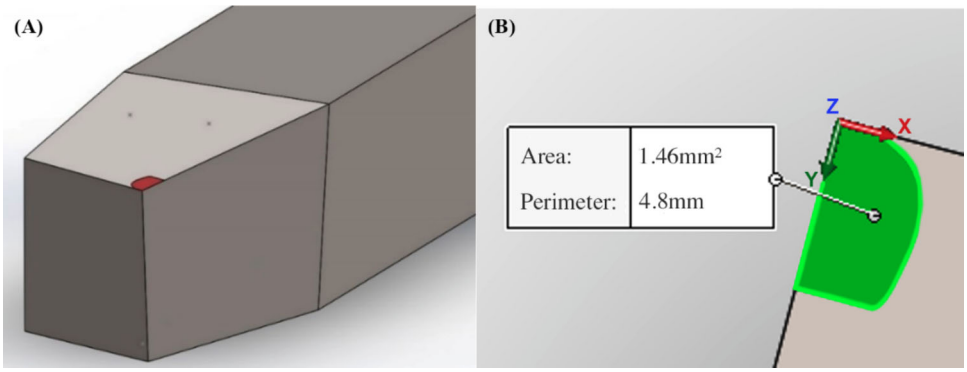

Fig. 3 **a** High-speed steel cutting tool for Case 1; **b** Zoomed wear region

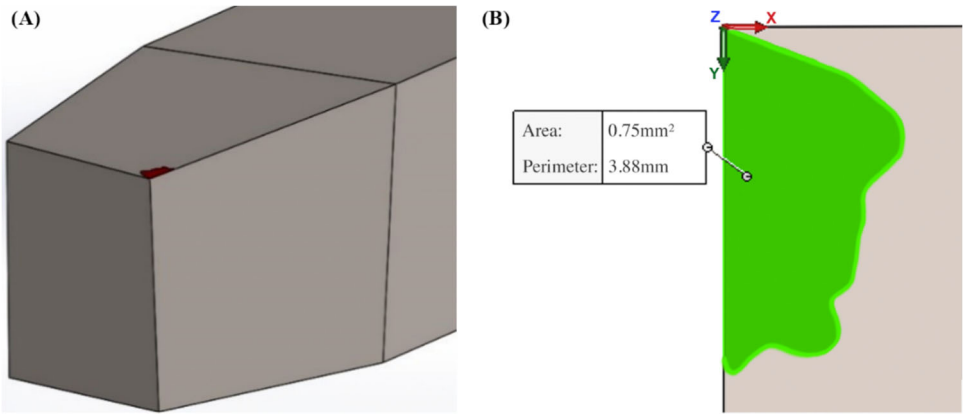

Fig. 4 **a** High-speed steel cutting tool for Case 2; **b** Zoomed wear region

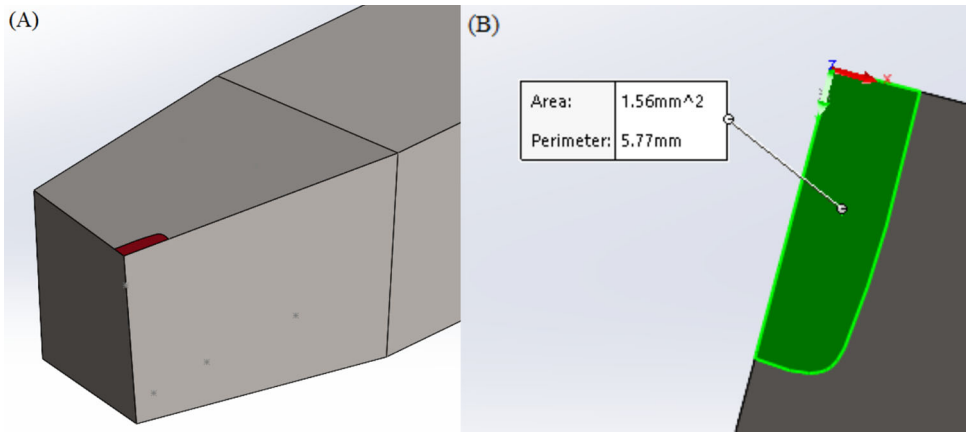

Fig. 5 **a** High-speed steel cutting tool for Case 3; **b** Zoomed wear region

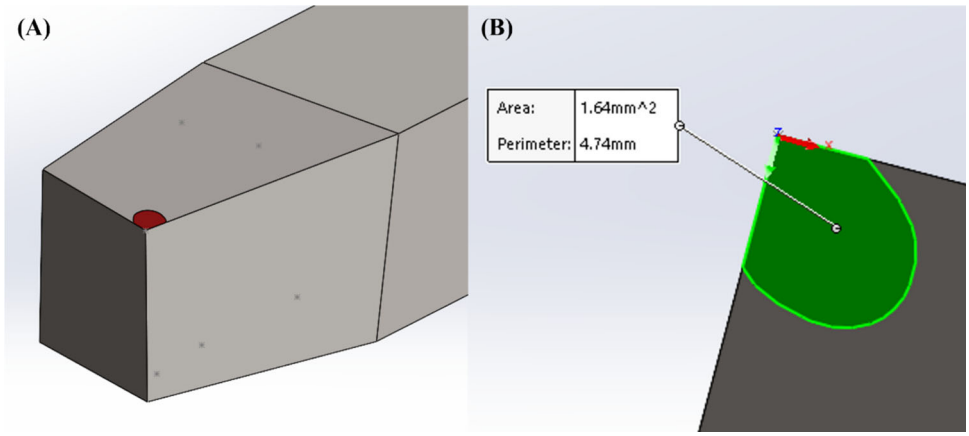

Fig. 6 **a** High-speed steel cutting tool Case 4; **b** Zoomed wear region

Table 1 Description of the cutting parameters for each case addressed in this work

Case	Cutting speed (m/min)	Depth of cut (mm)	Feed rate (mm/rev)
1	143	1.0	0.138
2	57	1.0	0.138
3	57	2.0	0.138
4	57	1.0	0.298
5	5	1.0	0.138

application. The Levenberg–Marquardt (LM) technique and the Finite Element Methodology (FEM) using COMSOL (Heat 2018) were selected among the three proposed numerical inverse techniques.

2.1 Analytical, numerical, and inverse techniques for solving the machining thermal problem

A methodology is used for estimating heat flux in cutting tools during the turning process. Such methodology is based on experimental temperature measurements in different regions of the tool. The problem analysis begins with the study of the cutting interface of the high-speed steel tool, as illustrated in Figs. 2, 3, 4, 5 and 6, which present CAD drawings of the high-speed steel cutting tool used in the experiment conducted by Santos et al. (2014) for the cases shown in Table 1.

The determination of the contact area is based on an analysis conducted after cutting is interrupted. The methodology involves measuring the contact area on three distinct edges of the cutting tool for each machining condition, enabling the calculation of an average value. For the measurement process, an image processing system is employed. Using a high-resolution video camera, the images obtained from the interrupted cutting process are analyzed and processed with the GLOBAL LAB Image software. This approach ensures

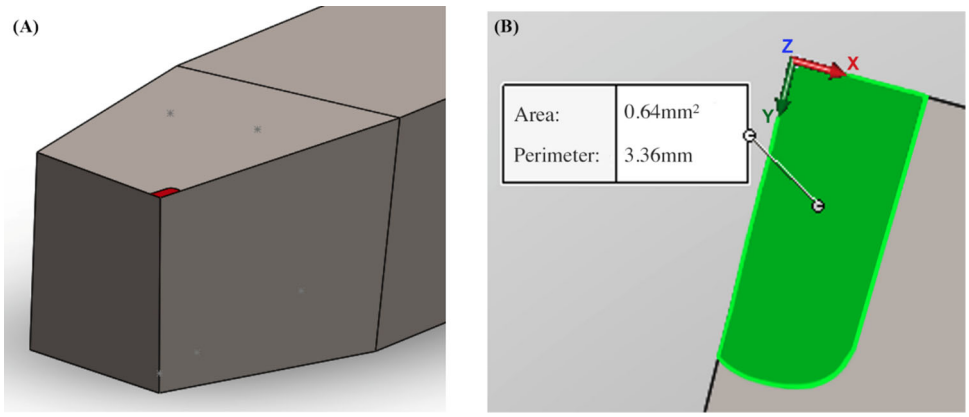

Fig. 7 **a** High-speed steel cutting tool for Case 5; **b** Zoomed wear region

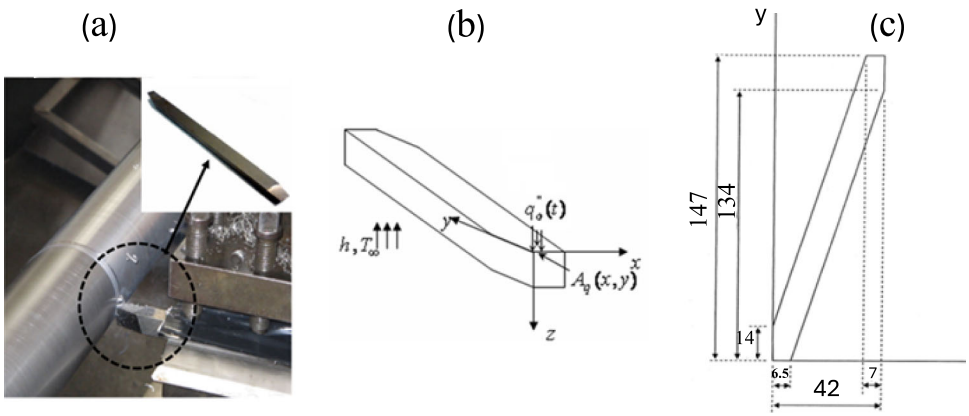

Fig. 8 **a** High-speed steel tool, **b** three-dimensional physical model, and **c** tool dimensions in millimeters (mm) where the coordinate "z" is 9.5 (mm). Source: Santos et al. (2014)

Table 2 Thermocouple Positions

Thermocouple	Coordinates on the cutting tool		
	X (mm)	Y (mm)	Z (mm)
1	6.1	7.2	0.0
3	0.0	9.0	5.0
4	3.3	7.0	8.098
5	2.0	3.4	8.098

Table 3 Specifications of the Tool Used in the Experiment

Specification	Value
Material	AISI M32C
Rake angle (%)	6°
Approach angle (%)	75°
Inclination angle (%)	0°
Nose angle (%)	90°
Relief angle (%)	8°
Nose radius	None

precise and reliable determination of the contact area under varying machining conditions.

According to Dourado da Silva et al. (2021), Santos et al. (2014), Erturk et al. (2023), and Lian et al. (2023). The thermal analysis developed in this paper is conducted in the rake face of the cutting tool, as presented in Figs. 3, 4, 5, 6, 7. The wear region is located in the rake face, and it generates the highest amount of heat flux.

Figure 8a shows the high-speed steel tool, while the cutting tool model used is presented in Fig. 8b. The dimensions of the tool are shown in Fig. 7c. The estimation of heat flux directly depends on the locations of the thermocouples. The interface contact area, denoted as $A_q\,(x, y)$, experiences the heat flux q" (x, y, t), due to contact between the tool and the workpiece. A constant convective heat transfer coefficient of 20 W/m^2 K is assumed on the remaining boundaries. Therefore, precise positioning of the thermocouples plays a fundamental role in solving inverse problems (Nosko 2024; Oliveira et al. 2022). Figure 8 and Table 2 provide the specific positions of the thermocouples in the experimental test conducted by Santos et al. (2014).

Table 3 presents the specifications of the cutting tool used in the study, offering a detailed description of its material and geometric parameters.

In Fig. 9, one may note the setup of the experiment conducted by Santos et al. (2014), with data obtained used for analysis in this study. The thermocouples shown in Fig. 9 are of T-type and are attached to the tool using the capacitive discharge method (Santos 2008). The experiment is performed on a conventional IMOR MAXI-II-520 – 6CV lathe. The experimental temperatures are recorded through an acquisition system named HP 75000 Series B data. It uses an E1326B voltmeter, controlled by a PC, as shown in Fig. 10.

The positioning of the thermocouples on the cutting tool, located at the coordinates described in Table 2, can be viewed in Fig. 11.

The thermal problem is governed by the 3D transient heat diffusion Eq. (1), as shown by Santos et al. (2014), where T is the temperature, λ is the thermal conductivity, and $\rho.Cp$ is the product of density and specific heat capacity.

$$\frac{\partial}{\partial x}\left(\lambda.\frac{\partial T}{\partial x}\right)+\frac{\partial}{\partial y}\left(\lambda.\frac{\partial T}{\partial y}\right)+\frac{\partial}{\partial z}\left(\lambda.\frac{\partial T}{\partial z}\right)=(\rho.Cp).\frac{\partial T}{\partial t} \tag{1}$$

COMSOL Multiphysics 6.0 (Heat 2018) is used to approximate solution to direct and inverse problems. This software uses the finite element method to approach solution to a three-dimensional transient thermal model by employing an unstructured tetrahedral mesh. Moreover, it offers flexibility in adjusting boundary conditions and models the geometry under study. Hence, the representation and discretization of the investigated system are illustrated in Fig. 12.

Similarly to Figs. 12 and 13 shows the tetrahedral mesh, which is automatically dimensioned by COMSOL Software (Heat 2018). Such mesh is applied to the cemented carbide cutting tool used for analyzing the three optimization techniques, which is previously described in the solution of the direct heat transfer problem.

For the models developed so far, the choice of tetrahedral mesh is due, not only to its straightforward computational implementation, but also to its ability to adapt to complex geometries. Case 4 is taken to carry out a mesh convergence test. Taking into consideration the advantages, previously mentioned, the maximum temperature percentual deviation for each thermocouple demonstrates that a mesh with around 6952 elements is appropriate, as shown in Fig. 12.

The goal of a thermal inverse technique is to estimate the transient heat flux for each machining experiment. This parameter must be determined in such a way that the resulting effect matches the experimental data or exhibits the least possible discrepancy from these data.

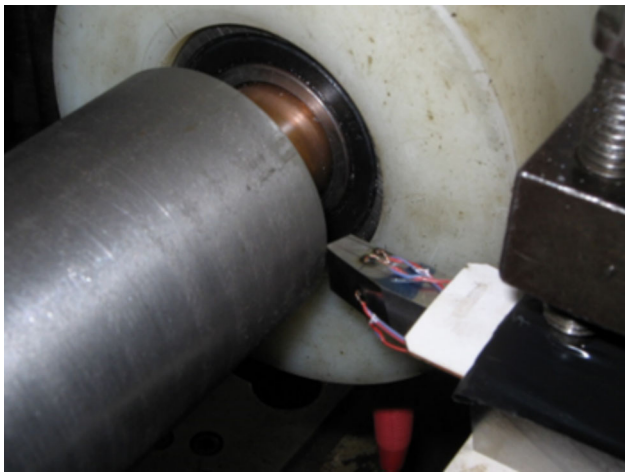

Fig. 9 Photo of the experiment conducted by Santos et al. (2014). Source: Santos (2008)

Fig. 10 Equipment setup used during the experiment conducted by Santos et al. (2014). Source: Santos (2008)

The Levenberg–Marquardt (LM), Nelder-Mead (NM), and Linear Specified Function (LSF) are numerical optimization techniques that are widely utilized in mechanical engineering (Levenberg 1944a; Marquardt 1963; Nelder and Mead 1965a; Lawson and Hanson 1974). The LM method integrates gradient-descent and Gauss–Newton methods. It efficiently solves nonlinear least squares problems by iteratively updating parameters to minimize residual errors. The LM method approaches gradient information from the Jacobian matrix (Levenberg 1944a; Marquardt 1963). The LM method is appropriate when applied to problems characterized by smooth, continuous, and differentiable functions. This ensures rapid convergence through gradient-informed adjustments.

On the other hand, the NM method employs direct search optimization without requiring gradient computations (Nelder and Mead 1965a). Based on simplex geometry, NM

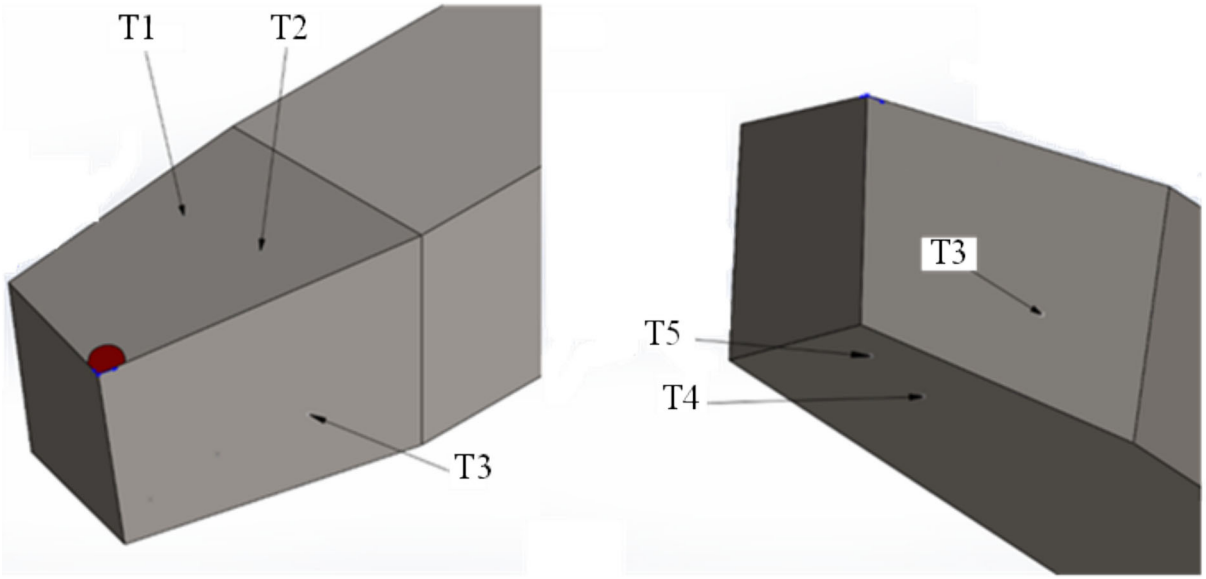

Fig. 11 Position of the thermocouples on the cutting tool

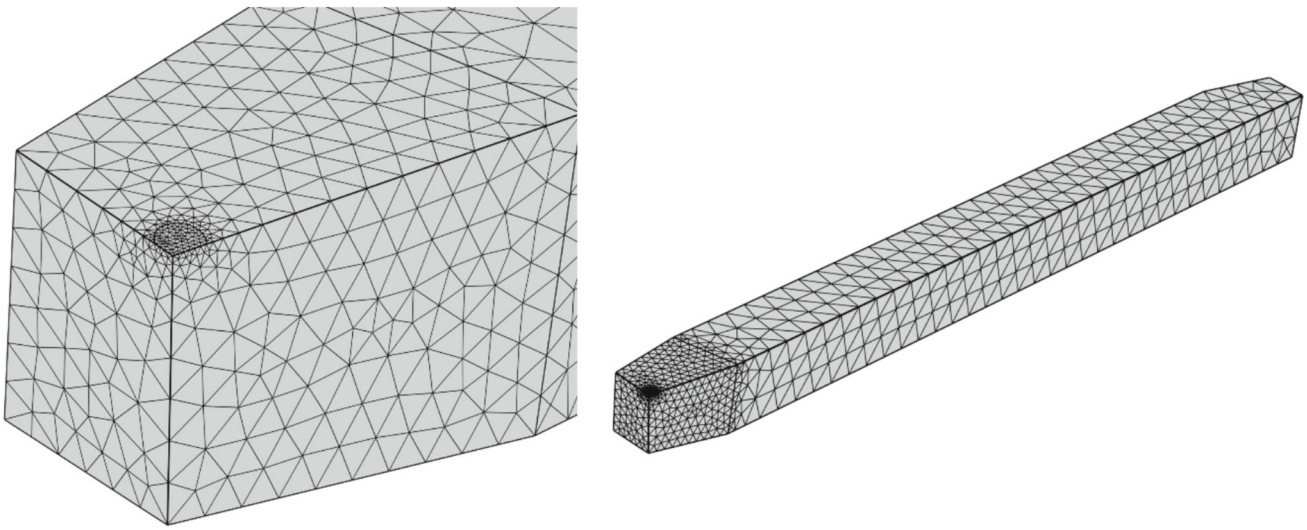

Fig. 12 The cutting tool domain with tetrahedral mesh with 6952 elements in Case 4

iteratively evaluates and adjusts vertices within a multidimensional simplex to locate function minima. This gradient-free approach is particularly effective for complex, noisy, or discontinuous objective functions. It offers robustness where derivative information is unreliable or unavailable.

The Linear Specified Function (LSF) method iteratively approximates unknown parameters through piecewise linear functions (Lawson and Hanson 1974). Being significantly valuable in inverse heat transfer analyses, the LSF method mitigates the drawbacks inherent in such problems by enforcing linear constraints. Such method reduces sensitivity to measure noise and enhances stability.

In this work, the objective function from by Lima e Silva et al. (2015), is adopted in Eq. (2):

$$F = \sum_{i=1}^{ns} (T_{exp}(x,\ y,\ z,\ t)_p - T_{num}(x,\ y,\ z,\ t)_p)^2 \tag{2}$$

In Eq. (2), F is the objective function, T_{exp} is the experimental temperature, T_{num} is the numerically calculated temperature, ns is the number of sensors used, and p is the index denoting the p^{th} sensor employed.

The primary goal of solving inverse problems is to minimize the objective function to find the optimal value of heat flux. In this context, three techniques are tested: Linear Specified Function (LSF), Levenberg–Marquardt (LM),

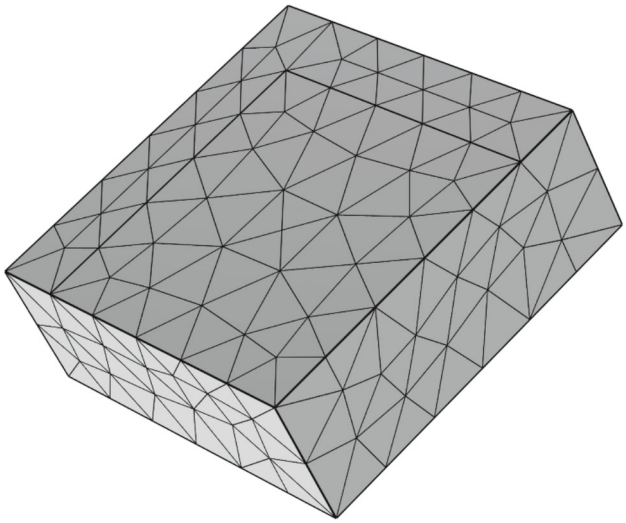

Fig. 13 Tetrahedral mesh applied to the cemented carbide cutting tool for validation of the direct heat transfer problem

and Nelder-Mead (NM). A detailed analysis of these techniques is conducted to determine which technique offers the best cost–benefit ratio for tackling inverse problems.

LSF, Beck et al. (1985) inherently incorporates a minimization process of the objective function. They employ components of heat flux to estimate time-dependent surface heat flux. Besides, LM (Zhenwu et al. 2022; Bergou et al. 2020; Hanke 1997; Levenberg 1944b; Marquardt 1962; Golsorkhi and Tehrani 2014) combines elements from the Steepest Descent and Gauss–Newton methods in order to seek for a numerical approximation to minimize the nonlinear function. NM (McKinnon 1999; Yu 1979a, b; Kolda et al. 2003; Lewis et al. 2007; Nelder and Mead 1965b; Spendley et al. 1962; Marshall 1984) in turn, is based on the geometry of the problem and aims to optimize an objective function in a multi-dimensional space. The choice of the appropriate technique depends on specific demands from the inverse problem, ensuring the attainment of precise and effective results.

Figure 14 shows a flowchart, detailing the step-by-step LSF procedure. Similarly to Lima e Silva et al. (2015), it includes the inputs and outputs used to approach the inverse problem through the specified linear function.

The application of the Specified Function method in three-dimensional heat conduction, using MATLAB® and its developed algorithm, involves three distinct stages (Evaluate 2023).

In the first stage, the sensitivity coefficients must be calculated. For this, a simulation should be performed in COMSOL® Multiphysics, setting the heat flux to 1.0 Watt/m^2 on the contact area and the initial temperature throughout the computational domain to 0 °C (Levenberg 1944a). As a result, the sensitivity coefficients are obtained. These coefficients are equivalent to the temperatures obtained in °C in the COMSOL® Multiphysics. Therefore, these sensitivity coefficients are input data for the MATLAB® code containing the LSF (Evaluate 2023).

In the second stage, the inverse problem is solved by estimating the heat flux using experimental temperature data. The MATLAB algorithm takes into consideration experimental temperature in °C, thermocouple type and number, and subsequent time-step values (Evaluate 2023). It takes the sensitivity coefficients from the first stage and calculates the heat flux, ensuring precision in the inverse problem solution.

In the third stage, the estimated heat flux becomes an input to solve the direct problem, where COMSOL® Multiphysics is used to find the temperature field (Evaluate 2023). Inputs like thermophysical properties, boundary and initial conditions, and time-steps are also needed. It approximates solution to the heat diffusion equation and generates temperature data in comparison which will be contrasted with experimental measurements. By coupling MATLAB algorithm with COMSOL® Multiphysics, this comprehensive method ensures reliable estimation of heat flux and temperature distribution in mechanical engineering contexts (Levenberg 1944a; Evaluate 2023).

Levenberg–Marquardt and the Nelder-Mead method are part of the optimization package in COMSOL® Multiphysics (Beck et al. 1985), offering a robust approach to finding the optimal point for a wide range of functions. This feature makes it a valuable tool for solving various inverse problems and other models. However, it is important to note that Nelder-Mead may have a low convergence rate (Powell 1973; McKinnon 1999; Yu 1979a, 1979b; Kolda et al. 2003; Lewis et al. 2007; Nelder and Mead 1965b; Spendley et al. 1962).

Each of these techniques offers a unique approach to solving the inverse problem, allowing a thorough analysis to determine the most suitable one. It takes into consideration efficiency and performance in accordance with the available computing resources.

The study tackled uncertainties in heat flux measurement and power-to-heat conversion through meticulous experimental design and methodology. Potential errors, including measurement inaccuracies, are minimized by calibrating equipment and ensuring precise sensor placement. High-precision devices, such as K-type thermocouples, are used to improve accuracy and reduce uncertainties caused by interface resistance. A comprehensive error analysis is performed, emphasizing the mathematical model for thermal parameter estimation. Sensitivity analysis evaluates the impact of deviations in measured values, ensuring robust calculations. Additionally, inverse heat conduction techniques are validated against controlled scenarios to enhance reliability. The study contrasts experimental data with numerical modeling, concerning discrepancies and, therefore, achieving consistent results. This dual approach ensures effective cross-validation and reduces uncertainty impact on conclusions.

This process provides a reliable framework for accurate thermal analysis.

3 Results and discussion

In turning machine processes, it is unreasonable to directly measure heat flux due to the physical conditions and system arrangement, which involve direct contact between the workpiece and the cutting tool. This makes it impossible to include any device for measuring heat flux in this interface. Therefore, an alternative methodology for validation is the creation of a controlled experiment in which flux and temperature are measured on the cutting tool (Carvalho et al. 2006).

The present study utilizes experimental data from Santos et al. (2014). In this work, a laboratory experiment is conducted to measure and obtain experimental heat fluxes and temperatures using two thermocouples. This controlled experiment is employed to validate the numerical data obtained using COMSOL® Multiphysics. In a subsequent experiment conducted by Santos et al. (2014), their experimental results are utilized to evaluate three numerical inverse techniques using the console and MATLAB®. The controlled experiment is conducted to measure experimental heat flux with the objective of validating numerical inverse techniques.

Subsequently, these variables are compared over time, allowing for the analysis of variations presented by the technique used in relation to the controlled experiment. This procedure enables the identification of the advantages and disadvantages of each technique and the selection of the most suitable one for solving thermal problems in machining.

3.1 Thermal model

The next step of this work involves the analysis and validation of the three inverse techniques presented. For this validation, the controlled experiment is used to validate the direct problem. In general, in this validation process, experimental temperatures T01 and T02 is provided as inputs to each inverse method to estimate heat flux. Subsequently, the estimated fluxes are compared with the experimental flux, as illustrated in Fig. 15.

When analyzing Fig. 15, it can be observed that all three techniques provide satisfactory results in estimating heat flux, closely approaching the experimental result. Additionally, Fig. 16a and b illustrate good agreement between the numerically estimated temperatures by each technique and the experimental temperatures recorded by Thermocouples T01 and T02. It is important to note that, for the purpose of experiment validation, the heat flux and estimated temperatures are considered only within the period in which the heater in the experiment was on, in other words, up to 63.27 s, as heat loss to the system is uncontrolled.

For a more detailed analysis of the temperature comparison, the residuals between numerical and experimental data are presented in Fig. 17a and b. In the case of the Nelder-Mead method, no deviations are plotted due to the high computational cost required by this technique, which requires

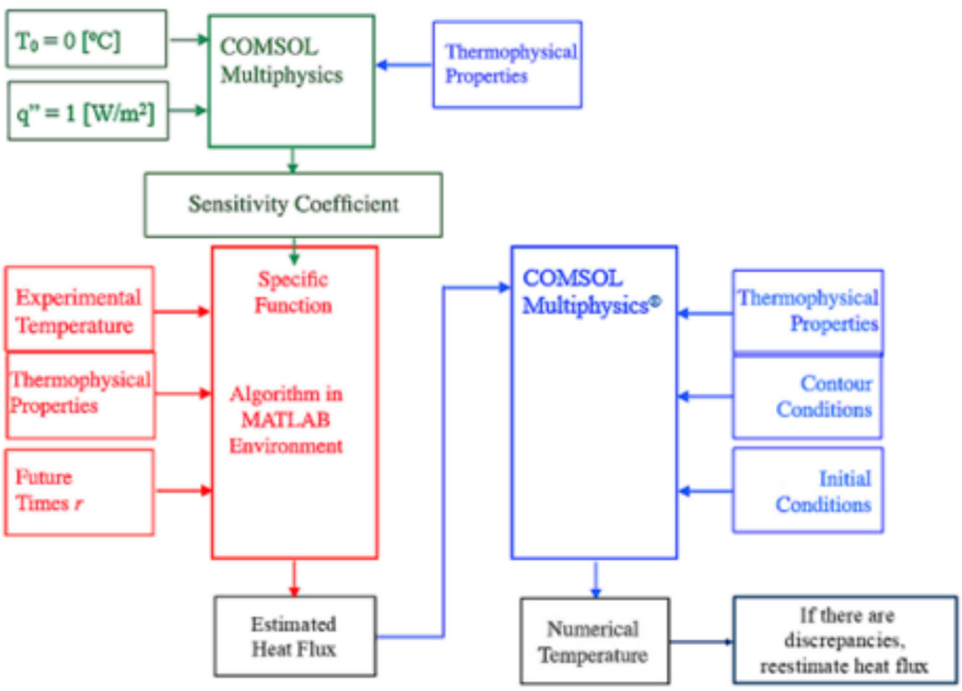

Fig. 14 Scheme for the use of the specified linear function

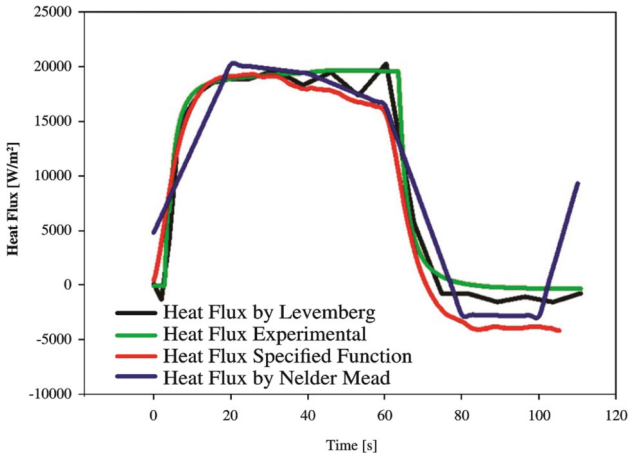

Fig. 15 Comparison of experimental and estimated heat flux by the 3 techniques LSF, LM, and NM

significant adjustments to the time step and consequently further increase in simulation time. It is observed that, during the effective period, temperature residuals do not exceed 3 °C, indicating good agreement between numerical and experimental data for the LM and LSF methods.

A relevant aspect in choosing the best method among those presented is the computational cost associated with each technique in solving the inverse validation problem. Table 3 compares the computational time spent by each technique. It is evident that the Nelder-Mead method demands significantly more computational time, rendering it unfeasible for use in solving the problems proposed in this work.

Therefore, considering Table 4, Figs. 11 and 12, the technique selected as the most suitable is the Levenberg—Marquardt method due to its low computational cost and

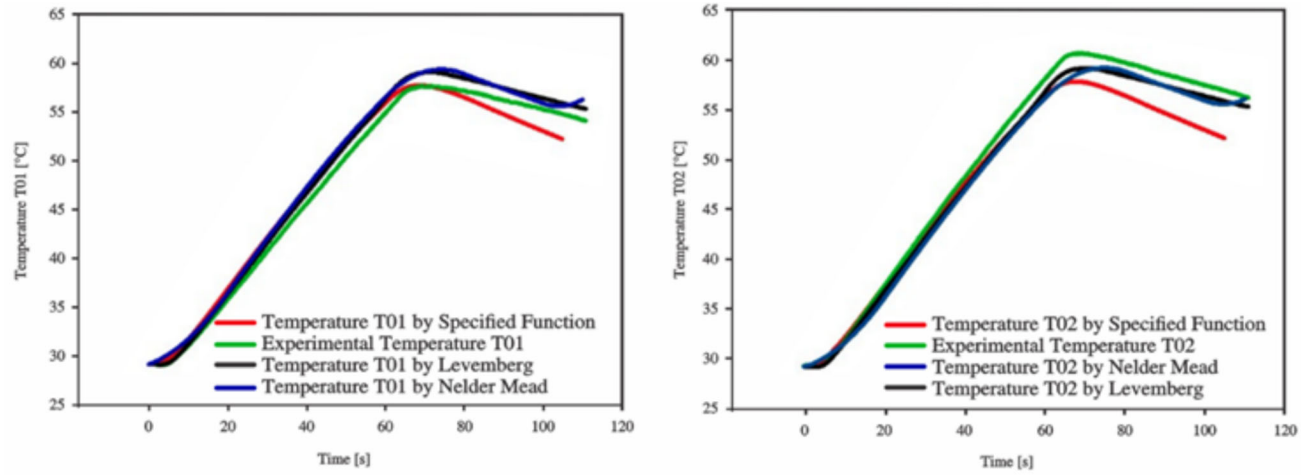

Fig. 16 Comparison of numerical temperatures obtained through estimated fluxes for each technique and the experimental ones: **a** Thermocouple T01; **b** Thermocouple T02

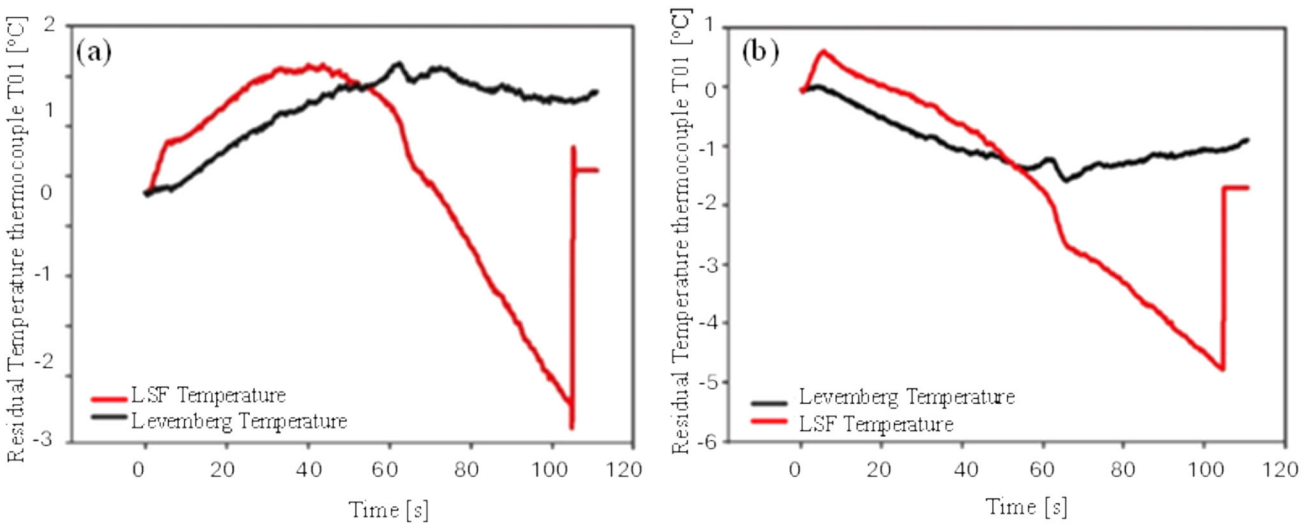

Fig. 17 Residual temperature between LM and LSF regarding experimental data for: **a** Thermocouple T01; **b** Thermocouple T02

Table 4 Computational time spent solving the inverse problem by each technique

Ranking	Inverse technique	Computational time spent [min]
1	Levenberg–Marquardt	5
2°	Linear specified function	5
3°	Nelder-Mead	4441

excellent temperature estimates, which closely match the experimental temperatures.

An additional advantage of the Levenberg–Marquardt method is its practicality, as the entire modeling and resolution process can be performed directly in the COMSOL software (Beck et al. 1985). On the other hand, the Linear Specified Function technique requires integration between two software tools, MATLAB® and COMSOL® (Heat 2018; Evaluate 2023), to solve the inverse problem. Its algorithm is written in the MATLAB environment, which uses experimental temperature data to estimate heat flux through the minimization of an objective function. With the heat flux curve obtained, this data is subsequently incorporated into COMSOL® (Heat 2018) to obtain the estimated temperatures based on that heat flux. The complexity of this integration and the computational cost involved make Levenberg–Marquardt the most suitable choice for solving the thermal problems in machining addressed in this study.

3.2 Heat flux and temperature estimation using Levenberg–Marquardt

To validate and determine the number of tetrahedral elements that compose the mesh used in the finite element method employed by COMSOL® Multiphysics, a study is conducted to compare computational time and the percentage temperature deviation found between the different mesh configurations, ranging from 2564 to 42,388 finite elements. The results obtained will be presented in chapter 3.3.

The results of the heat flux and temperature estimations are obtained by applying the Levenberg–Marquardt technique as a method for minimizing an objective function to solve the inverse problems. The results of the estimations for the mentioned variables are presented for three different workpiece rotational cases: 900 RPM, 355 RPM, and 28 RPM. Additionally, the comparison between the results of the heat flux and temperature estimations are given for depth of cut and feed rate variation. For 355 RPM rotation, the comparison is between 1.0 and 2.0 mm depth of cut and between 0.138 and 0.298 mm/rev, regarding cutting parameter cases shown in Table 5.

The model, based on the geometric and physical characteristics of the experiments conducted by Santos et al. (2014), is built and discretized in the COMSOL Multiphysics 6.0 software. The temporal aspects of the model are discretized to represent the actual experiment conditions, with a time interval of 0.112 s for storing output data. The total duration of the experiment is 126.224 s, resulting in 1128 measurements and data storage points throughout the experiment. For Case 4, the total duration of the experiment is 87.248 s, covering all the effective machining time, which meets the objective of this study. It is relevant to note that the experiment is conducted at an average room temperature (25 °C) right from the beginning. Also, the cooling system operates under natural air convection.

3.3 Finite elements mesh configuration study for Levenberg–Marquardt technique

For the present study, an analysis of the computational mesh to be used in thermal simulations with the commercial software COMSOL® (Heat 2018) is conducted. The results of this analysis are presented in the following sections. The analysis is performed on a computer equipped with an Intel® Xeon W-1250 processor at 3.30 GHz, 64 GB of RAM, and an integrated Intel® UHD Graphics GPU. Case 4 is chosen to obtain the percentage deviation results between the experimental temperatures from Santos et al. (2014) and those numerically obtained. The different mesh configurations and their corresponding results are shown in Table 5 and Fig. 18.

Figure 18 shows the relationship between the number of finite elements and both the computational time and the greatest percentage deviation in thermocouple readings (T03, T04, and T05). The results demonstrate that as the mesh density increases, the percentage deviation stabilizes, indicating convergence while computational time rises significantly. This analysis ensures that the selected mesh provides a balance between accuracy and computational efficiency.

According to the comparison of the results presented in Table 5 and Fig. 18, it is observed that the mesh configuration containing 6952 finite elements provides the best balance between computational time cost and result accuracy (Heat 2018). This approach reflects upon the maximum percentage deviation of the temperatures obtained numerically using the Levenberg–Marquardt optimization technique compared to the experimental temperatures obtained by Santos et al. (2014). The mesh with 6952 elements delivers the same quality of results as the mesh containing 42,388 tetrahedral elements, but requiring approximately 17 times less computational time. Therefore, the tetrahedral mesh containing 6952 finite elements is selected for cases 1–5.

Table 5 Results table for the analysis of the number of elements in the tetrahedral mesh

Finite elements mesh quantity	Computational time spent	Thermocouple T03 greatest percentage deviation	Thermocouple T04 greatest percentage deviation	Thermocouple T05 greatest percentage deviation
2564	15 min 15 s	2.1592	1.4047	0.5925
3180	21 min 1 s	2.1589	1.3849	0.6018
6952	38 min 32 s	2.1375	1.3805	0.5869
9351	1 h 11 min 37 s	2.1399	1.3886	0.5840
12,541	1 h 32 min 18 s	2.1387	1.3839	0.5854
42,388	10 h 38 min 27 s	2.1383	1.3805	0.5880

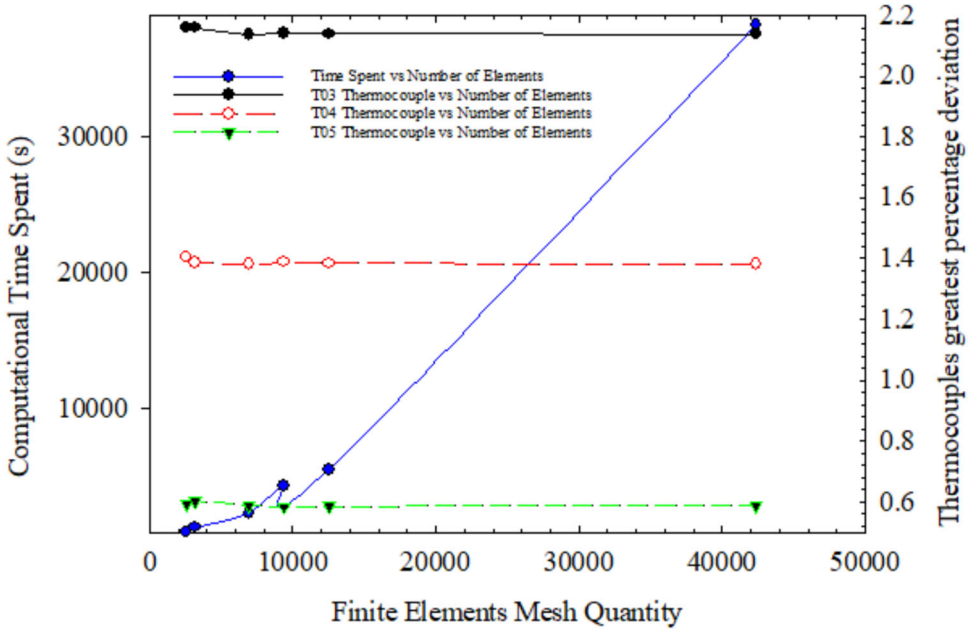

Fig. 18 Convergence graphical analysis of the number of elements in the tetrahedral mesh

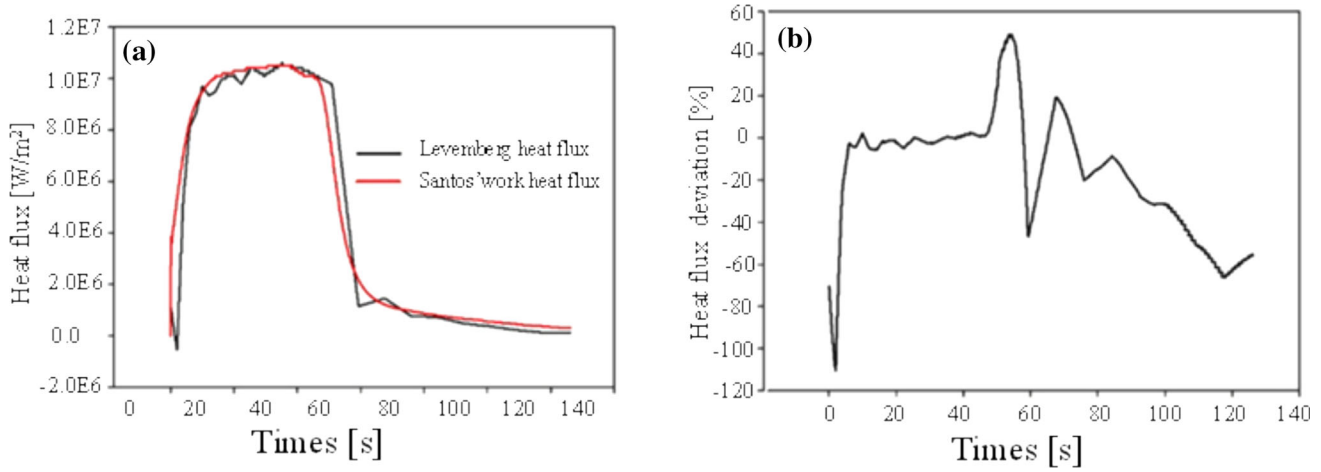

Fig. 19 **a** Comparison between the heat flux estimated by Levenberg and the flux estimated by Santos et al. (2014) for Case 1; **b** Percentage deviation between the estimated fluxes by Santos et al. (2014)

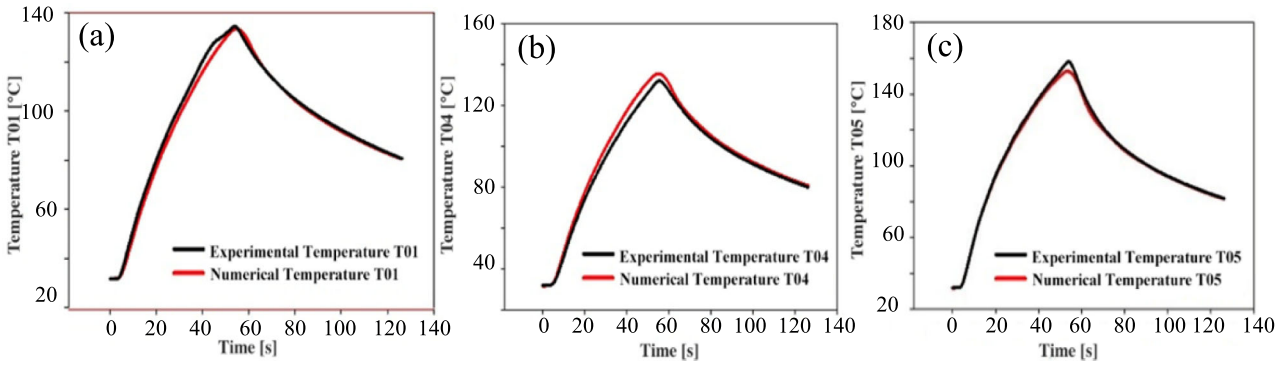

Fig. 20 Comparison between the numerical temperatures obtained by Levenberg–Marquardt and the experimental temperatures from Santos et al. (Lima e Silva et al. 2015). **a** Thermocouple T01; **b** Thermocouple T04; **c** Thermocouple T05

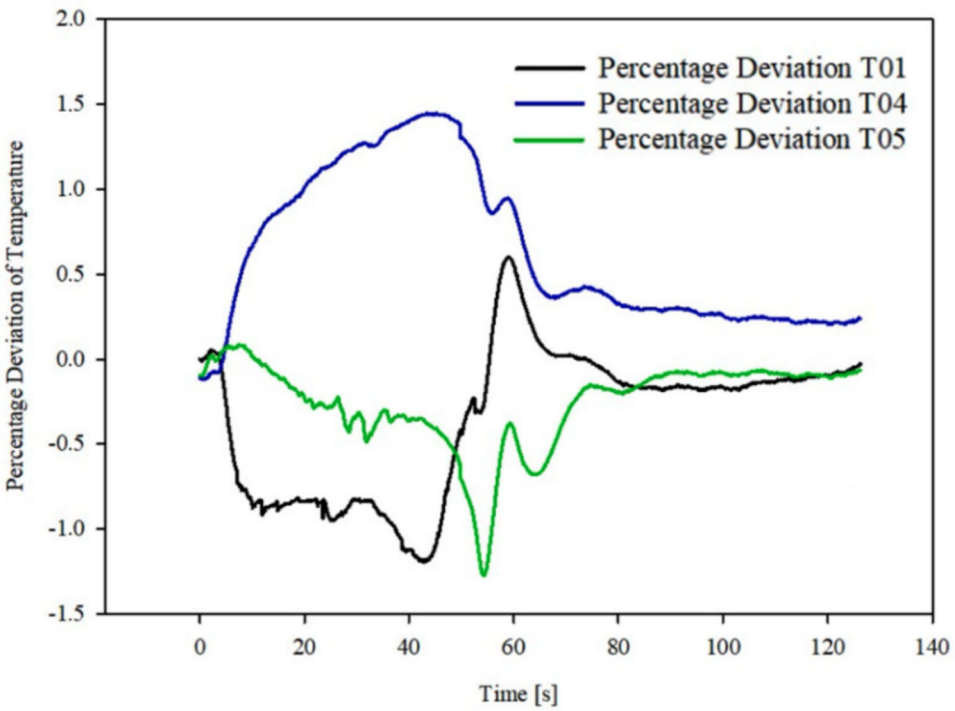

Fig. 21 Comparison between the numerical temperatures obtained by Levenberg–Marquardt and the experimental temperatures from Santos et al. (Santos and Lima e Silva et al. 2014).
a Thermocouple T01;
b Thermocouple T04;
c Thermocouple T05

3.4 Results corresponding to case 1–900 RPM, 1.0 mm depth of cut and 0.138 mm/rev feed rate

In Fig. 18a, the heat flux estimations obtained using the Levenberg–Marquardt method are presented along with the estimated values from the study conducted by Santos et al. (2014), which employs the Inverse 3D technique to estimate heat flux using the function specification method. An evident agreement between these estimations over time can be observed, as illustrated in Fig. 18a. Figure 18b shows the percentage deviation of the estimated heat flux from this study compared to that of Santos et al. (2014).

By examining Fig. 19b, it can be noted that during the effective cutting period, which extends to approximately 50 s, the percentage deviation remains at low levels. However, it increases as the cutting tool moves away from the machining point.

As a result of the model developed in the COMSOL software (Heat 2018), graphs representing the estimated temperatures throughout the machining period are generated, taking into consideration the heat flux estimated by the applied technique for solving the inverse problem. In Fig. 20, a comparison is presented between the experimental temperatures obtained from Santos et al. (Lima e Silva et al. 2015) research and the estimated temperatures at the measuring points of thermocouples T01, T04, and T05. This comparison considers the heat flux estimated using the Levenberg–Marquardt method.

It is relevant to highlight that for all the scenarios analyzed, the results prove to be highly satisfactory, as shown in

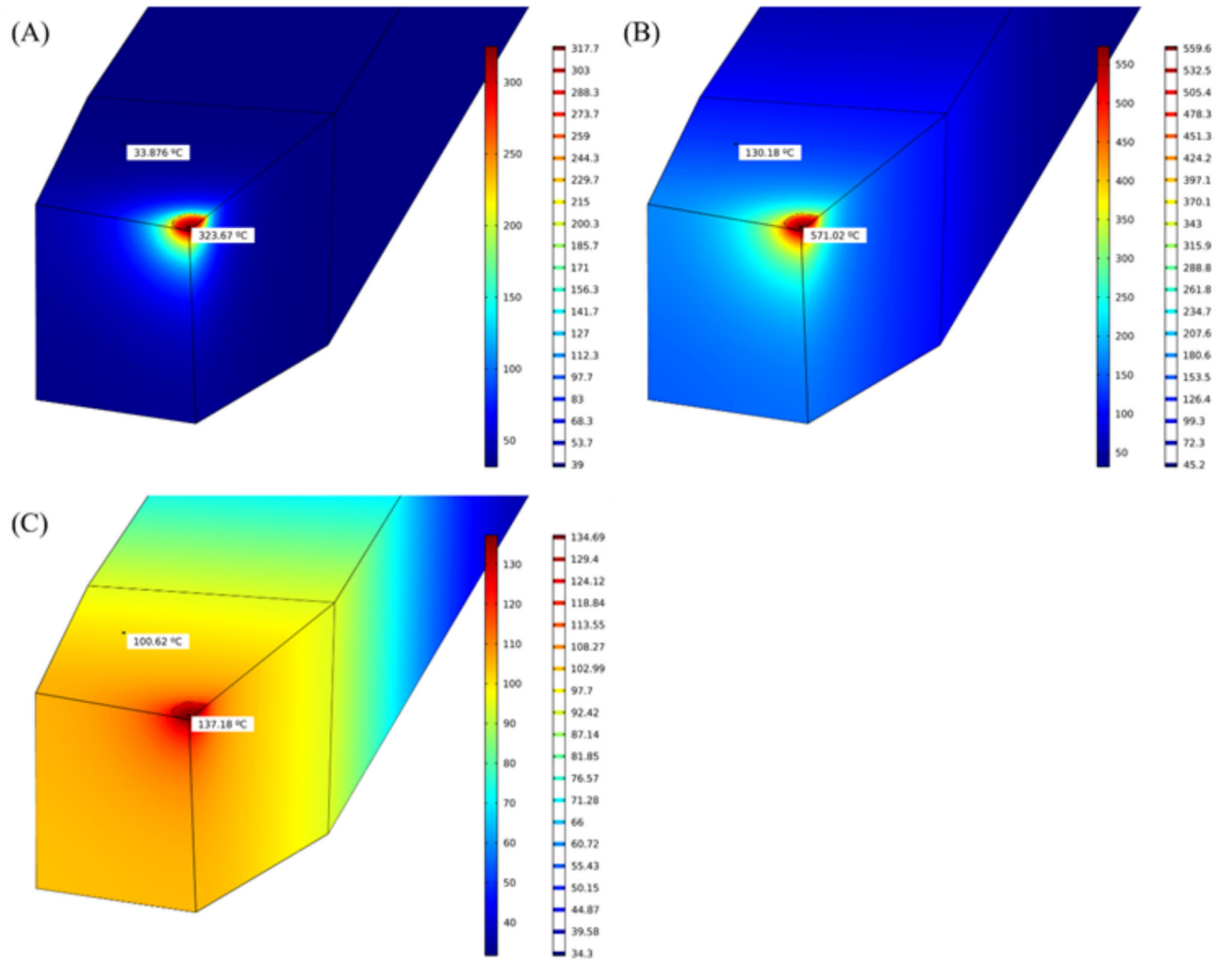

Fig. 22 Temperature field on the cutting tool for Case 1: **a** t = 5 s; **b** t = 50 s; **c** t = 85 s

Fig. 21. The estimated temperatures demonstrate a significant agreement to the experimental temperatures throughout the machining process. In Fig. 21, the percentage deviation between the estimated temperatures and the experimental temperatures can be observed. It is important to note that the maximum deviation does not exceed 1.5%, an exceptional value that validates the method effectiveness even under high-speed conditions.

Once the distribution of heat flux and the temperature field on the cutting tool are established (Fig. 22), understanding the thermal behavior in the tool wear region is of significance. This region is considered critical due to its elevated temperatures and wear rate. The resolution of the inverse problem allows the estimation of temperatures at various points in this critical region. Figure 22 illustrates the evolution of the temperature field on the cutting tool at relevant moments of the machining process. The temperature is measured at a specific point located in the wear region, and its behavior is evaluated in the initial stages of machining, when the cutting tool loses contact with the workpiece, as well as in moments after the process.

Figure 22 depicts that in the 50 s of the machining process, the cutting tool under analysis exhibits a significant thermal gradient, reaching temperatures exceeding 570 °C while machining.

Regarding the wear region, the behavior of maximum, average, and minimum temperatures in this area is recorded throughout the machining process. For each time interval, the corresponding temperatures are monitored by the COMSOL® software (Bergou et al. 2020), allowing for the creation of the graph presented in Fig. 23.

The information presented in Fig. 23 is relevant for predicting temperatures in the wear region. In the context of this study, direct experimental temperature measurements in this area are impractical. This is primarily because the region experiences continuous contact between the workpiece and

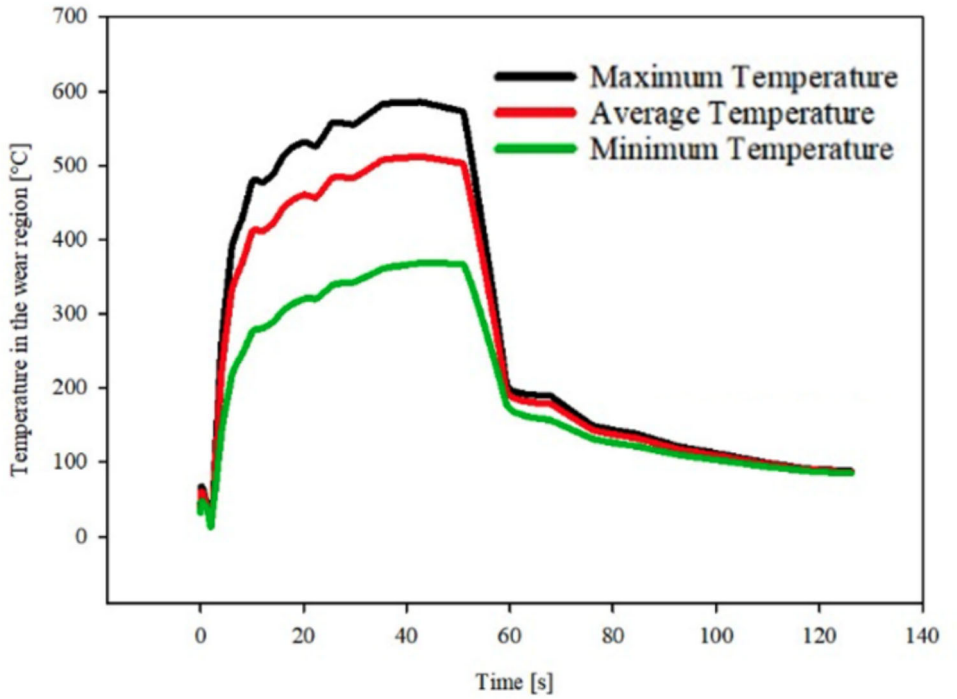

Fig. 23 Maximum, average, and minimum temperatures in the wear region

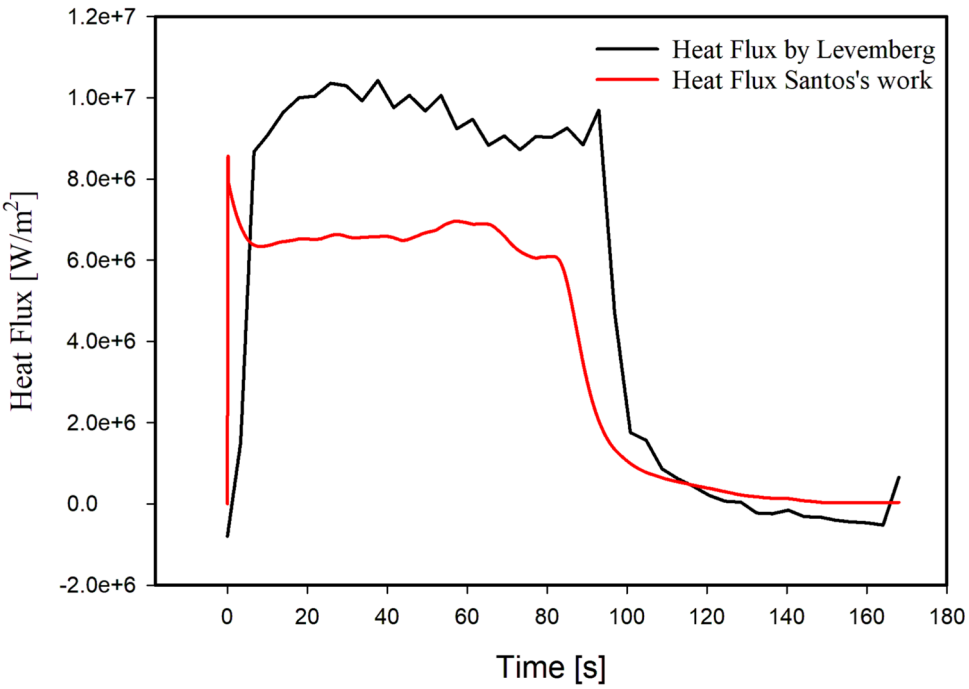

Fig. 24 Comparison between the heat flux estimated by Levenberg and the flux estimated in the study by Santos et al. (2014) for Case 2

the cutting tool. Additionally, there is constant chip generation on the cutting tool surface.

3.5 Results corresponding to case 2 – 355RPM, 1.0 mm depth of cut and 0.138 mm/rev feed rate

The comparison between the heat flux estimated by COMSOL (Beck et al. 1985) and the flux estimated by Santos et al. (2014) is presented in Fig. 24.

In Fig. 25, for Case 2, the heat flux estimated by COMSOL® exhibits substantial deviations compared to

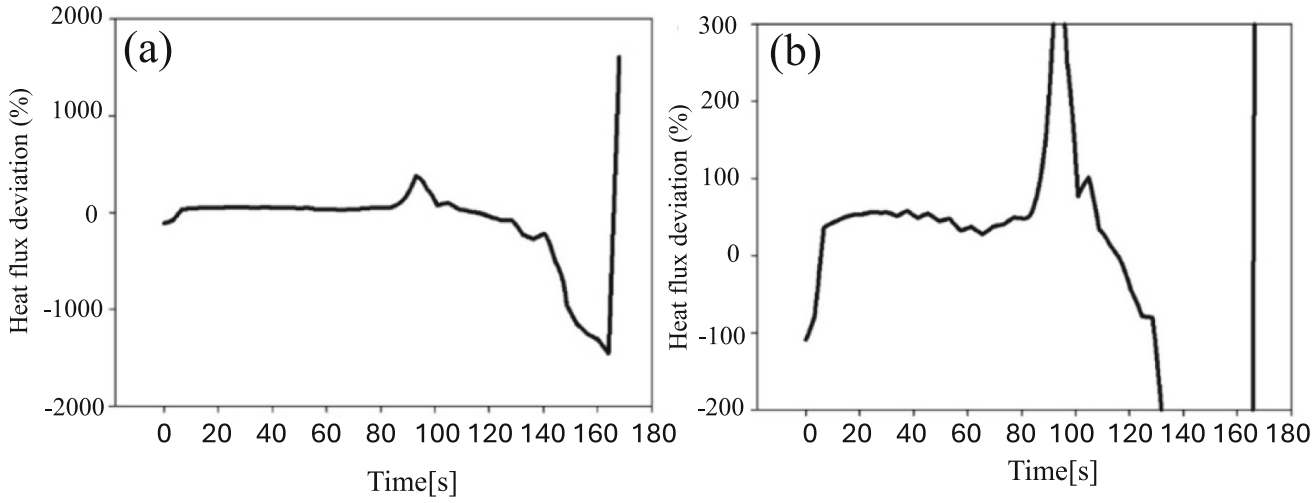

Fig. 25 Percentage deviations of heat flux; **a** overall view of the curve throughout the test; **b** zoomed-in curve emphasizing the cutting period

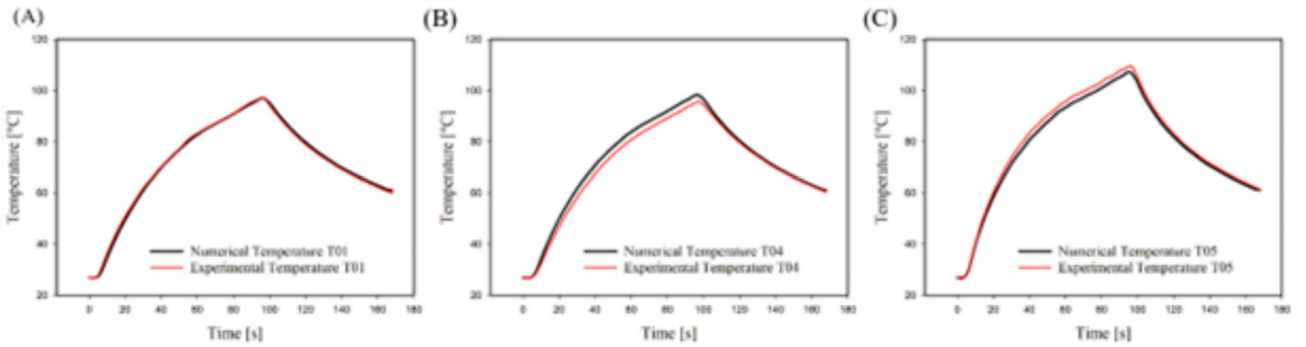

Fig. 26 Comparison between the numerical temperatures obtained by Levenberg–Marquardt and the experimental temperatures from Santos MR et al. (Marquardt 1963). **a** Thermocouple T01; **b** Thermocouple T04; **c** Thermocouple T05

those from Santos et al. (2014) and Beck et al. (1985). These discrepancies can be analyzed in terms of percentages through the curves presented in Fig. 25a and b. Figure 25a provides an overall view of the percentage deviations throughout the entire test, while Fig. 25b emphasizes the cutting period, thus highlighting the discrepancies during this specific stage of the process.

The machining time for this case is approximately 90 s. During this period, the heat flux exhibits an average percentage deviation of 45.20%, a value higher than the average deviation observed in the cutting interval for Case 1, which is around 7%. However, it is worth noting that the estimated temperatures obtained from this heat flux estimated by the Levenberg–Marquardt (LM) method show agreement with experimental data, for all three thermocouples considered as Fig. 26 shows.

The analysis of Fig. 26 reveals alignment between the curves for thermocouples T01, T04, and T05. This is contradictory given the results obtained in the heat flux comparison shown in Fig. 25. However, considering the similarity between the results presented in Case 1 and the other cases, the data are deemed valid for further analyses and comparisons between the findings.

The close alignment of the temperatures shown in Fig. 26 is confirmed by the analysis of Fig. 27, which presents the percentage deviations between the temperatures estimated numerically using COMSOL® and the experimental temperatures reported by Santos et al. (2014). The maximum percentage deviations found for thermocouples T01, T04, and T05 are 0.6%, 1.0%, and 0.8%, respectively, reflecting the accuracy of the Levenberg–Marquardt optimization method.

Figure 28 shows the progression of the temperature field on the cutting tool at significant moments during the machining process, in parallel with Case 1. Due to the characteristics of the experiment conducted by Santos et al. (2014), the times selected to obtain the 3D temperature field of the cutting tool are adjusted in Fig. 28 compared to Fig. 22. The purpose of this adjustment is to capture the largest temperature changes during machining, allowing for a clearer understanding of the experiment progression. This adjustment scenario also applies to subsequent cases.

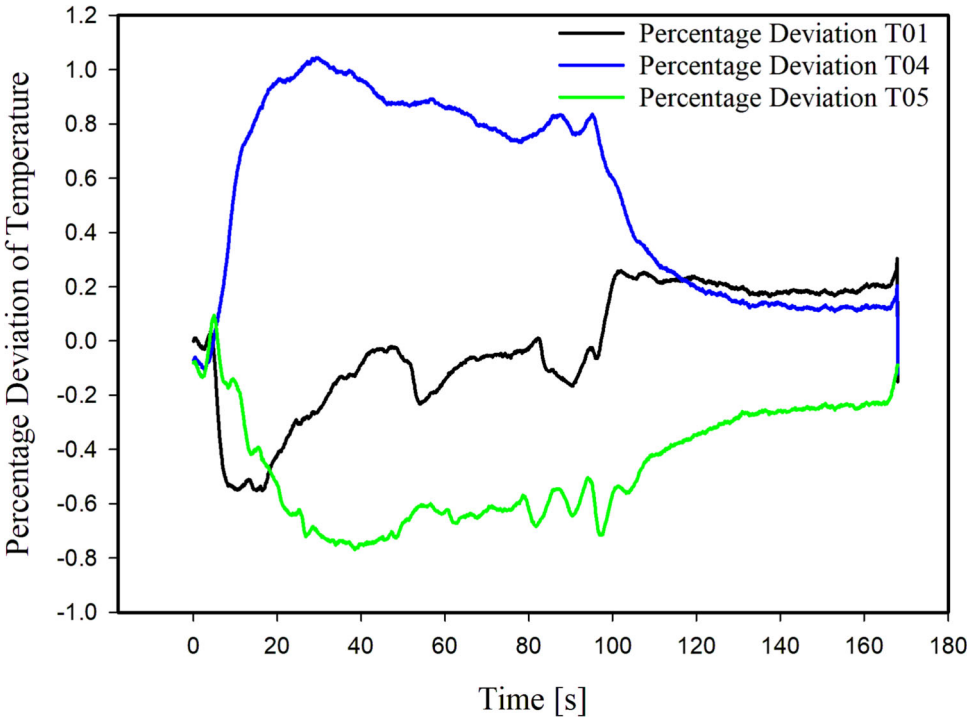

Fig. 27 Percentage temperature deviations obtained through the comparison between the numerical temperatures obtained by Levenberg–Marquardt and the experimental temperatures from Santos et al. (2014) for Thermocouples T01, T04, and T05

It can be pointed out in Fig. 28b that, at 90 s into the process, the cutting tool under analysis exhibits a significant thermal gradient, reaching a temperature of 400 °C at the highest point of heat generation in this case. Compared to Case 1, it is observed that the maximum temperature exceeds the one found for Case 2, as shown in Fig. 28b. This is explained by the difference in the cutting parameter rotation: 900 RPM for Case 1 and 355 RPM for Case 2, resulting in a more severe cutting configuration in Case 1 and, consequently, greater heat generation (Diniz et al. 2005).

As evidenced in Fig. 29, similarly to the Case 1 scenario, the estimation of maximum, average, and minimum temperatures in the wear region is conducted for Case 2.

After examining Fig. 29, it is possible to estimate that the maximum temperature remains around 400 °C for severe conditions of the machining process. Once again, it is noteworthy that this maximum temperature is lower when compared to Case 1, in which high rotation resulted in temperatures close to 600 °C. These results provide clear evidence that, as rotation increases, the temperature at the cutting interface tends to rise (Diniz et al. 2005).

3.6 Results corresponding to case 3 – 355RPM, 1.0 mm depth of cut and 0.298 mm/rev feed rate

The comparison between the heat flux estimated by COMSOL (Levenberg 1944a) and the flux estimated by Santos et al. (2014) is presented in Fig. 30.

A typical aspect of Case 3 is the shorter machining period considered in the graph generated. The analysis primarily focuses on the time when the tool is in contact with the workpiece and generating heat, representing the thermal effect under investigation. The temperature decrease phase is not accounted for in this evaluation. This characteristic is due to the difficulty in interpreting the thermocouple data acquisition beyond 90 s of temperature readings, resulting in the validation of temperature information only up to this point.

The analysis of Fig. 30a shows that the result obtained numerically using the Levenberg optimization method, compared to the experimental heat flux determined by Santos et al. (2014), exhibits similar values to real data from experimental approach. This similarity can be justified by examining Fig. 30b, which indicates reasonable average percentage deviation of 5.88% while the cutting tool is in contact with the workpiece, as shown in Fig. 31.

More temperature results for thermocouples T03, T04, and T05 from COMSOL® software are contrasted with the experimental temperatures recorded by Santos et al. (2014), as shown in Fig. 32. A slight deviation is observed for the temperatures of thermocouples T03 and T04. In contrast in Fig. 32, the deviation for thermocouple T05 is low. Figure 32 shows that for thermocouples T03 and T04, the percentage deviation of temperatures is higher, reaching maximum values of 2.14% and 1.38%, respectively. In contrast, the percentage deviation for thermocouple T05 is minimum and around 0.59%.

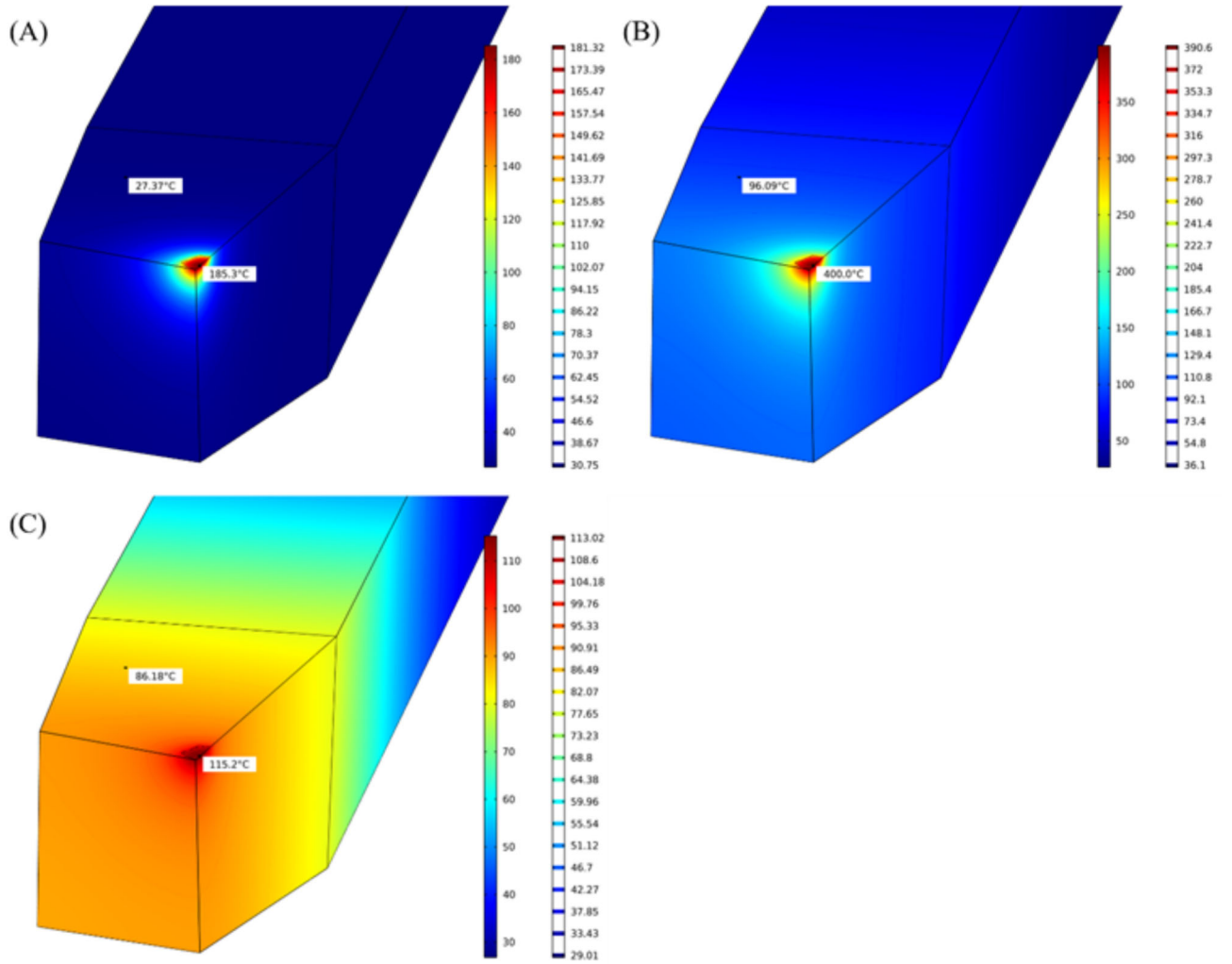

Fig. 28 Temperature field on the cutting tool for Case 2: **a** t = 5 s; **b** t = 90 s; **c** t = 110 s

It is noteworthy that Case 3 has some similarities to Case 2, whose machining parameters are presented in Table 1. The primary difference between them is the variation in the tool feed rate, from 0.138 to 0.298 mm/rev. This change in the cutting parameter results in a more aggressive chip removal process, generating more heat (Diniz et al. 2005) and, consequently, increasing the tool temperature. This statement is verified by comparing Figs. 28b and 33b, which show that for the machining times corresponding to the temperature peaks at the cutting interface (90 s and 50 s, respectively, for Cases 2 and 3), the temperature difference exceeds 130 °C in Case 3, indicating a more severe cutting depth.

Figure 33a shows that during the first 5 s of machining, there is a considerable increase in the temperature at the cutting interface compared to its surroundings. Additionally, it is observed that the temperature at the cutting interface reaches a significant value of 537 °C. The temperature fields presented are obtained using the COMSOL® Multiphysics software (Heat 2018) and exhibit high-quality representation.

Specifically at the tool cutting interface, the maximum, average, and minimum temperatures are depicted in Fig. 34, supporting the results previously presented.

3.7 Results corresponding to case 4 – 355RPM, 2.0 mm depth of cut and 0.138 mm/rev feed rate

The heat flux results obtained numerically using the Levenberg–Marquardt optimization technique for Case 4 are presented in Fig. 35, along with the heat flux estimated by Santos et al. (2014).

Figure 35 shows that, initially, the heat flux estimated by Santos et al. (2014) exhibits a pronounced deviation, caused by temperature noise in the acquisition of experimental data. Subsequently, the heat flux estimated by the

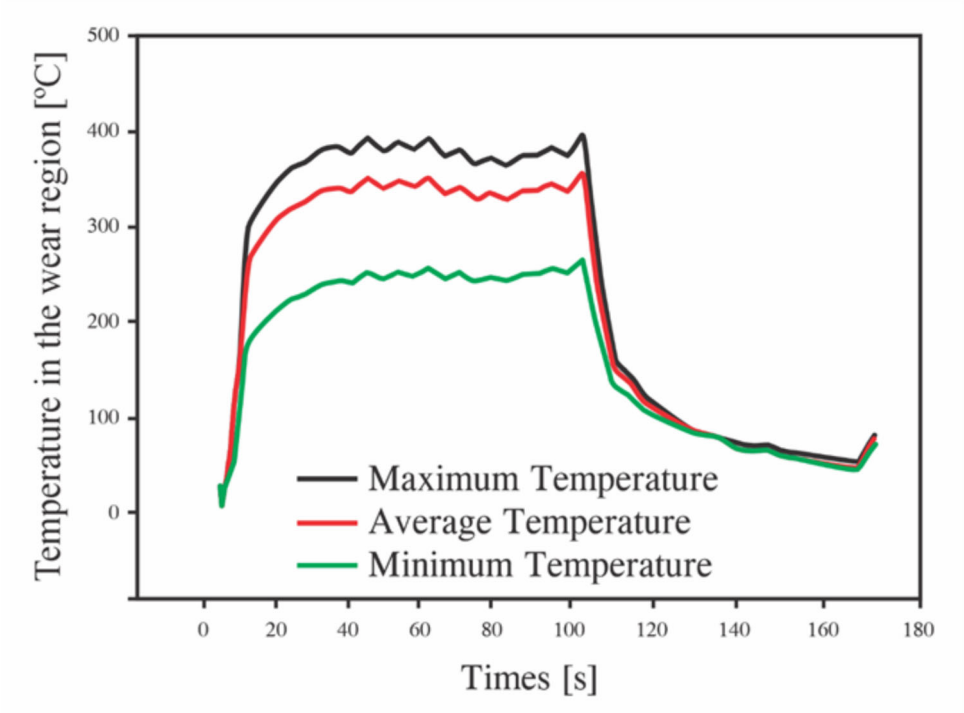

Fig. 29 Maximum, average, and minimum temperatures in the wear region for Case 2

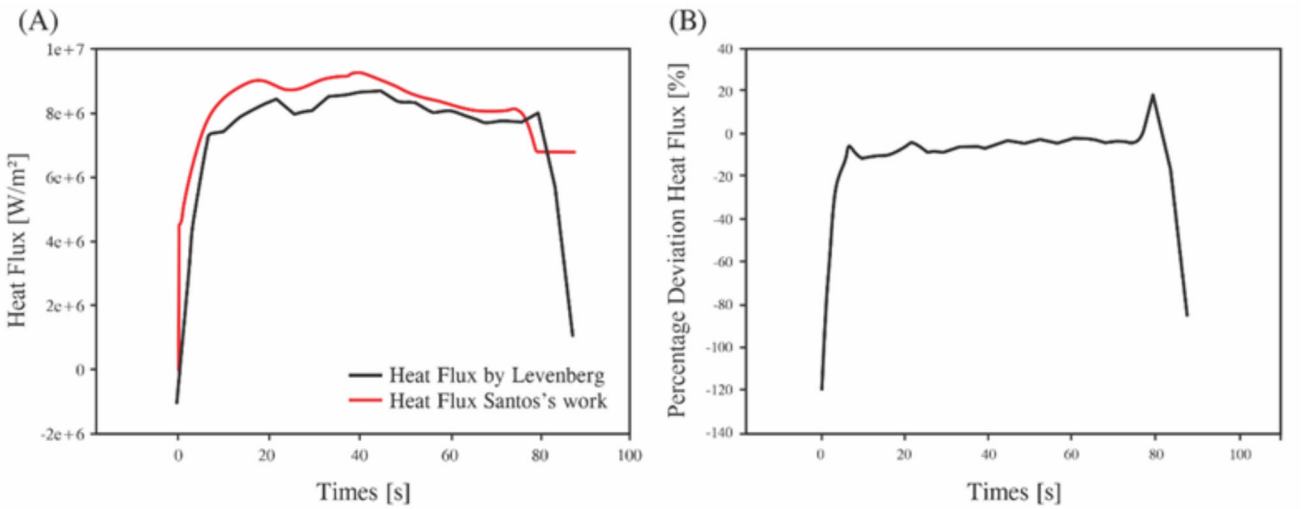

Fig. 30 **a** Comparison between the heat flux estimated by Levemberg and the flux estimated by Santos et al. (2014) for Case 3. **b** Percentage deviation between the heat flux estimated by Levenberg and the flux estimated by Santos et al. (2014)

COMSOL software (Heat 2018) demonstrates good agreement, closely following the curve obtained by Santos et al. (2014). This close match is justified by the analysis of the percentage deviation between the heat fluxes, as presented in Fig. 36.

The analysis of Fig. 36a reveals that, from a broad perspective, the percentage deviation curve between the heat fluxes considered is extremely low and close to zero. Complementing this observation, Fig. 36b provides an expanded scale of the percentage deviation, allowing for the visualization of a slight percentage variation between the fluxes, with an average percentage deviation of 5.57% during the effective machining period, from 10 to 80 s. This value is considered acceptable for the simulation conditions.

As a result of the thermal model developed in the COMSOL software (Heat 2018), temperature curves calculated numerically for thermocouples T03, T04, and T05 are also obtained. These curves are compared with the experimental temperatures measured for the same thermocouples, as

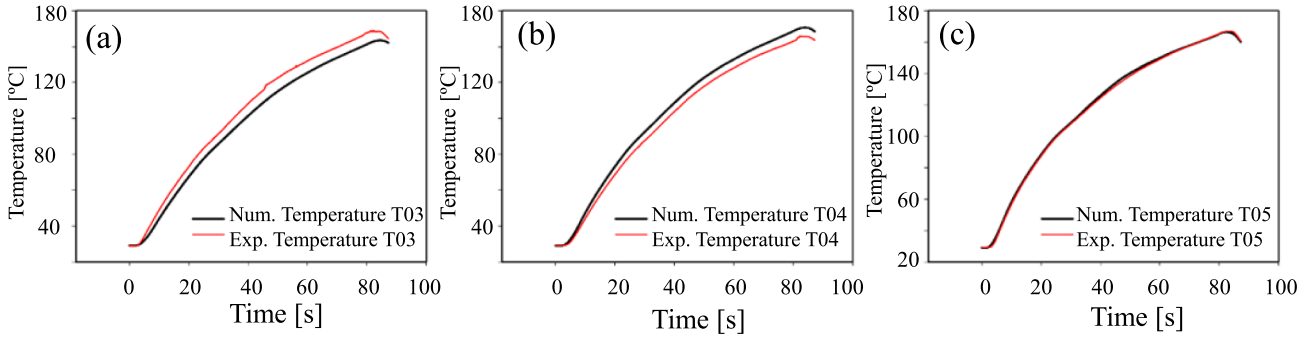

Fig. 31 Comparison between the numerical temperatures obtained by Levenberg–Marquardt and the experimental temperatures from Santos et al. (2014). **a** Thermocouple T03; **b** Thermocouple T04; **c** Thermocouple T05

reported in the study by Santos et al. (2014). This comparison is presented in Fig. 37.

The analysis of Fig. 37a and b, corresponding to thermocouples T03 and T04, respectively, reveals a small deviation between the temperatures obtained numerically using the commercial COMSOL software (Heat 2018) with the Levenberg–Marquardt optimization technique and the experimental temperatures (Santos et al. 2014). In the case of Fig. 37c, corresponding to thermocouple T05, the temperatures are identical, making it visually impossible to detect any relative deviation.

The close agreement between the temperatures shown in Fig. 37 is confirmed by the analysis of Fig. 38.

Figure 38 presents the percentage deviation between the temperatures obtained numerically and experimentally. It can be observed consistency with previous temperature analysis that thermocouples T03, and T04 show higher percentage deviations compared to thermocouple T05. This premise is confirmed by the maximum percentage deviation observed for each thermocouple: 1.86% for T03 and 1.37% for T04. These results are better compared to the percentage deviations obtained for Case 3. For thermocouple T05, a maximum percentage deviation of only 0.5% is found, which explains the notable similarity between the temperature curves in Fig. 37c.

Similarly to the comparison made between Cases 3 and 2, it is also possible to compare the temperature results obtained for Cases 4 and 2. The cutting depth parameter differs between Cases 2 and 4, varying from 1.0 to 2.0 mm, respectively. In other words, the cutting parameters for Case 4 are considered more severe than those for Case 2, resulting in increased heat generation (Diniz et al. 2005) and, consequently, higher temperatures. This can be clearly observed by comparing Figs. 28b and 39b, where at the machining time corresponding to the peak temperature during effective cutting, there is a temperature difference of 61.2 °C, with Case 4 being higher than Case 2.

As shown in Fig. 40 and similar to the cases discussed previously, the numerical simulation provided the estimated curves for the maximum, average, and minimum temperatures at the cutting interface for Case 4.

The analysis of Fig. 40 shows that the maximum temperature at the cutting interface reached 400 °C at the beginning of the machining experimental test and subsequently remained above 400 °C. This indicates a more intense heat generation compared to Case 2, as expected.

3.8 Results corresponding to case 5 – 28RPM, 1.0 mm depth of cut and 0.138 mm/rev feed rate

In Case 5, in Fig. 41, the machining time also extended to approximately 90 s. The comparison between the heat flux estimated by the Levenberg–Marquardt (LM) model and the flux estimated by Santos et al. (2014) shows small deviations when to one another.

Considering the effective cutting time, which is 90 s, it is observed that the average percentage deviation is around 2.27%, the lowest among the three cases (Fig. 42). In this scenario, it is remarkable that, for the severe condition of the machining process, the percentage deviation tends to remain constant. This behavior reflects a solid agreement between the flux estimated by the Levenberg–Marquardt (LM) method and the flux estimated in Santos et al.'s study (2014).

A comparative analysis between the temperatures estimated by the Levenberg–Marquardt (LM) method and the experimental measurements is presented for the three thermocouples in Fig. 43. Agreement between the estimates and measurements is observable for thermocouples T01, T04, and T05. All three thermocouples showed satisfactory results in terms of the deviation between the curves, as shown in Fig. 44, which displays the percentage deviation between the temperatures obtained numerically and those recorded in the experiment conducted by Santos et al. (2014).

The analysis of Fig. 44 shows that the percentage deviation between the compared temperatures is notably low. For thermocouples T01, T04, and T05, maximum percentage deviation values of 0.26%, 0.3%, and 0.18%, respectively, are

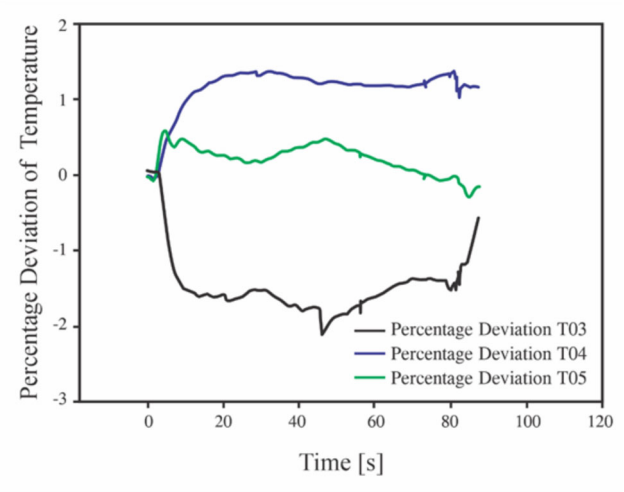

Fig. 32 Percentage Temperature Deviations obtained through the comparison between the numerical temperatures obtained by Levenberg–Marquardt and the experimental temperatures from Santos et al. (2014) for Thermocouples T03, T04, and T05

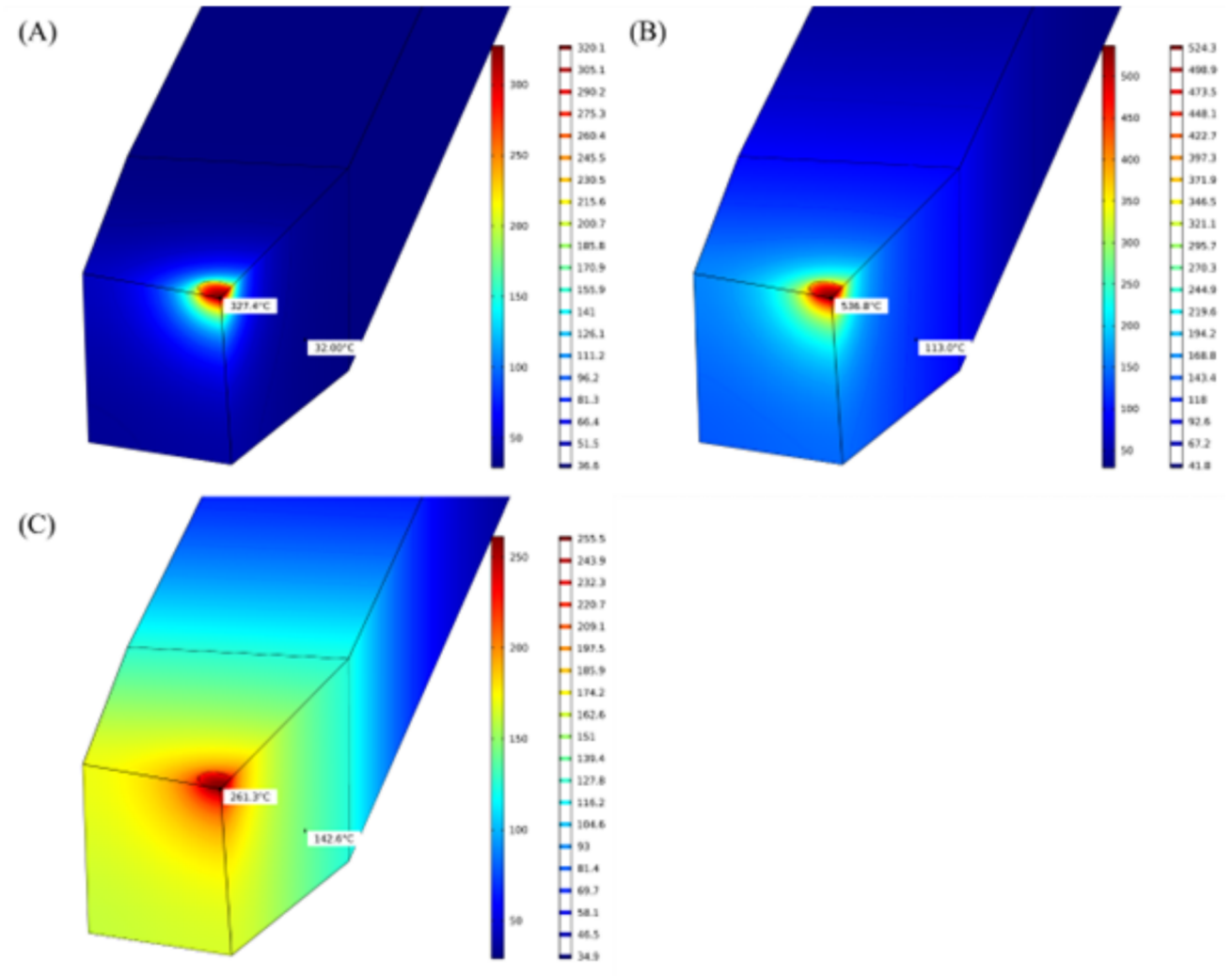

Fig. 33 Temperature field on the cutting tool for Case 3: **a** t = 5 s; **b** t = 50 s; **c** t = 85 s

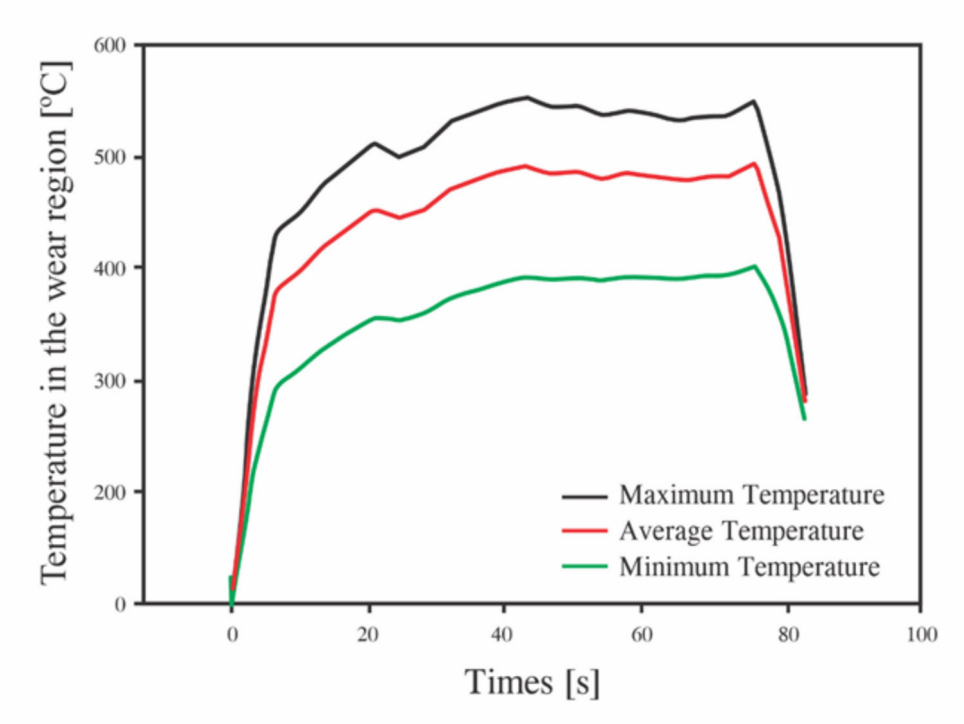

Fig. 34 Maximum, average, and minimum temperatures in the wear region for Case 3

found. This confirms the high degree of alignment between the temperature curves, ensuring greater reliability of the results obtained.

Figure 45 displays the evolution of the temperature field on the cutting tool at significant moments of the machining process, analogous to Case 1. It can be observed that the machining parameter settings for Case 1 exhibit a milder temperature distribution field compared to the previous cases. This is due to the more moderate cutting parameter configuration, resulting in lower heat generation than in the other cases (Diniz et al. 2005). Figure 45a and b show that the temperature increase at the cutting interface between 20 and 90 s is minimal, rising from 127 to 151 °C. This differs from previous cases, where temperature variation over similar machining times is significantly greater. For instance, in Case 3, the temperature increases from 327 to 537 °C °C between 5 and 50 s of machining, indicating a substantial temperature rise over a shorter effective machining period.

Maximum, average, and minimum temperatures are also estimated for the Case 5 scenario, as illustrated in Fig. 46. As expected, for the lowest rotation evaluated, the lowest temperatures are recorded among the three cases, not exceeding 160 °C in the wear region.

The results shown in Fig. 46 confirm the observation that, as the workpiece rotation rate increases, there is a corresponding rise in temperature within the wear region. Consequently, these elevated temperatures contribute to increased wear, primarily due to the reduction in material mechanical strength in response to the thermal effects (Fernández-Abia et al. 2011; Teixeira et al. 2023; Viale et al. 2002; Bergman et al. 2020; Luiz and Machado 2008; Grzesik 2017).

3.9 Comparison of studied cases (items 3.4 to 3.8)

Figure 47 presents the distributions of the maximum temperatures occurring in the cutting tool for Cases 1, 2, 3, 4, and 5, as follows:

Case 1 (900 RPM, Depth of Cut: 1.0 mm, Feed Rate: 0.138 mm/rev):

- This scenario exhibits the highest temperatures in the tool wear region, exceeding 570 °C.
- The elevated rotational speed (900 RPM) significantly increases heat generation at the cutting interface, resulting in higher thermal gradients and substantial heat dissipation.

Case 2 (355 RPM, Depth of Cut: 1.0 mm, Feed Rate: 0.138 mm/rev):

- Reducing the rotational speed decreased heat generation, leading to maximum temperatures around 400 °C.
- This case demonstrates a marked reduction in thermal impact compared to Case 1, highlighting the influence of rotational speed on heat generation.

Case 3 (355 RPM, Depth of Cut: 1.0 mm, Feed Rate: 0.298 mm/rev):

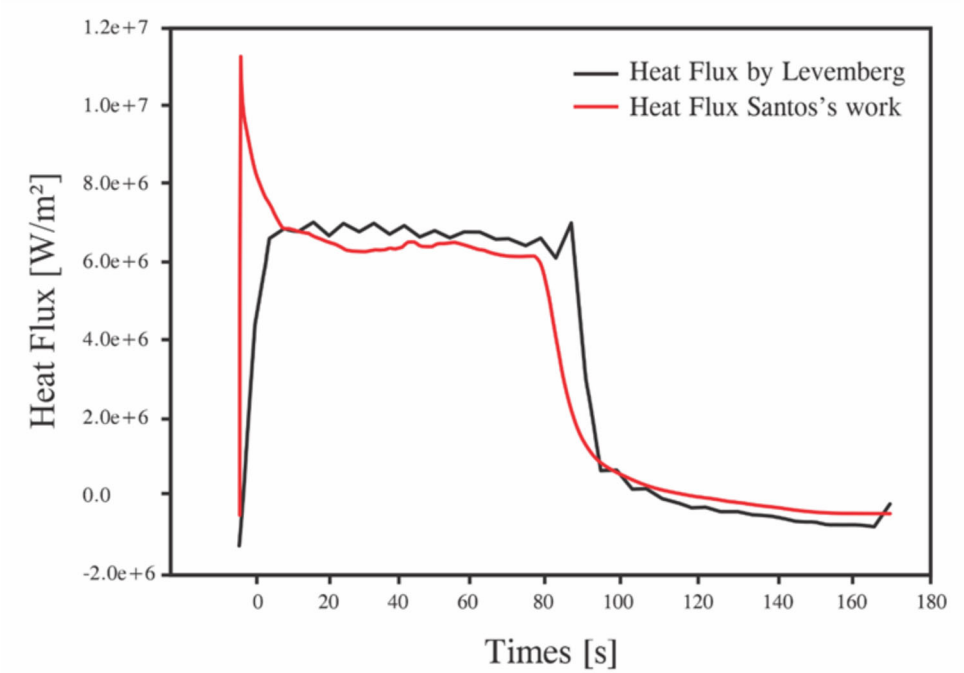

Fig. 35 Comparison between the heat flux estimated by Levenberg and the flux estimated in the study by Santos et al. (2014) for Case 4

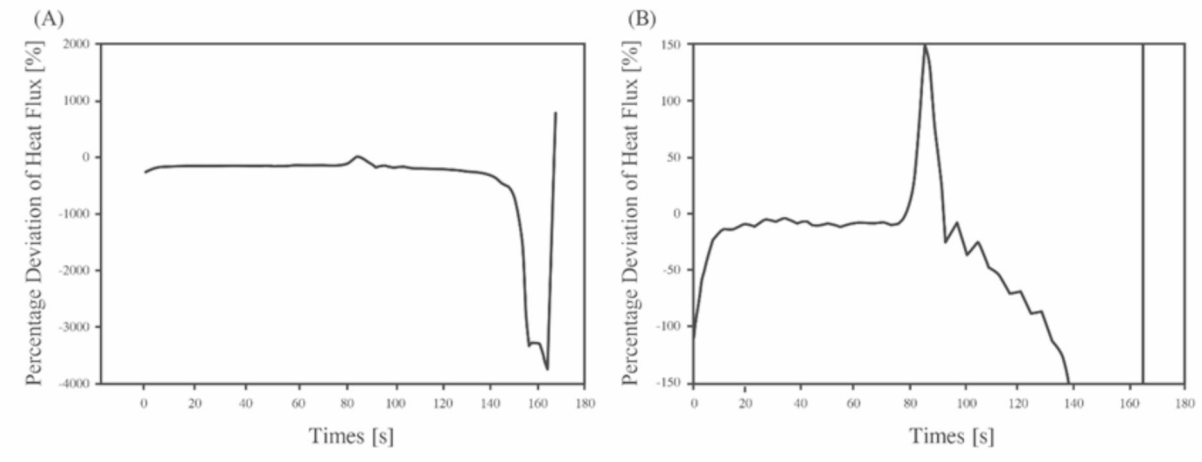

Fig. 36 Percentage deviations of heat flux for Case 4; **a** overall view of the curve throughout the test; **b** zoomed-in curve emphasizing the cutting period

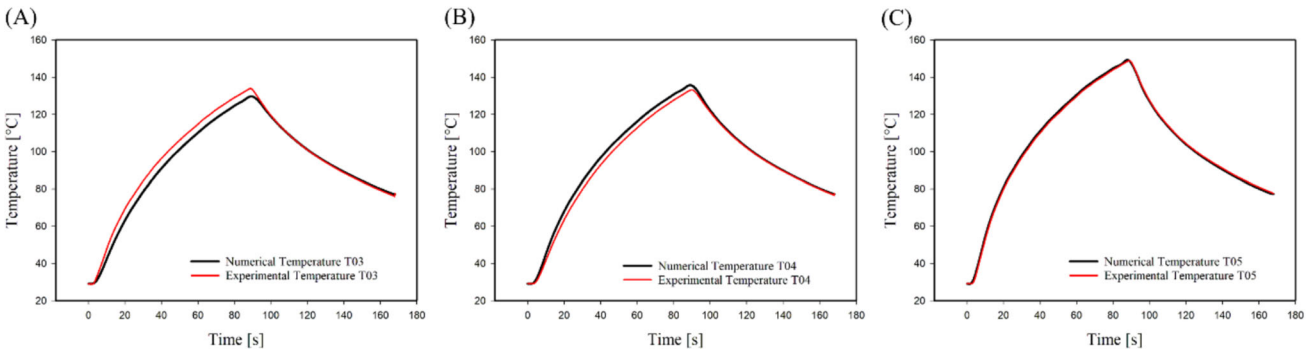

Fig. 37 Comparison between the numerical temperatures obtained by Levenberg–Marquardt and the experimental temperatures from Santos et al. (2014). **a** Thermocouple T03; **b** Thermocouple T04; **c** Thermocouple T05

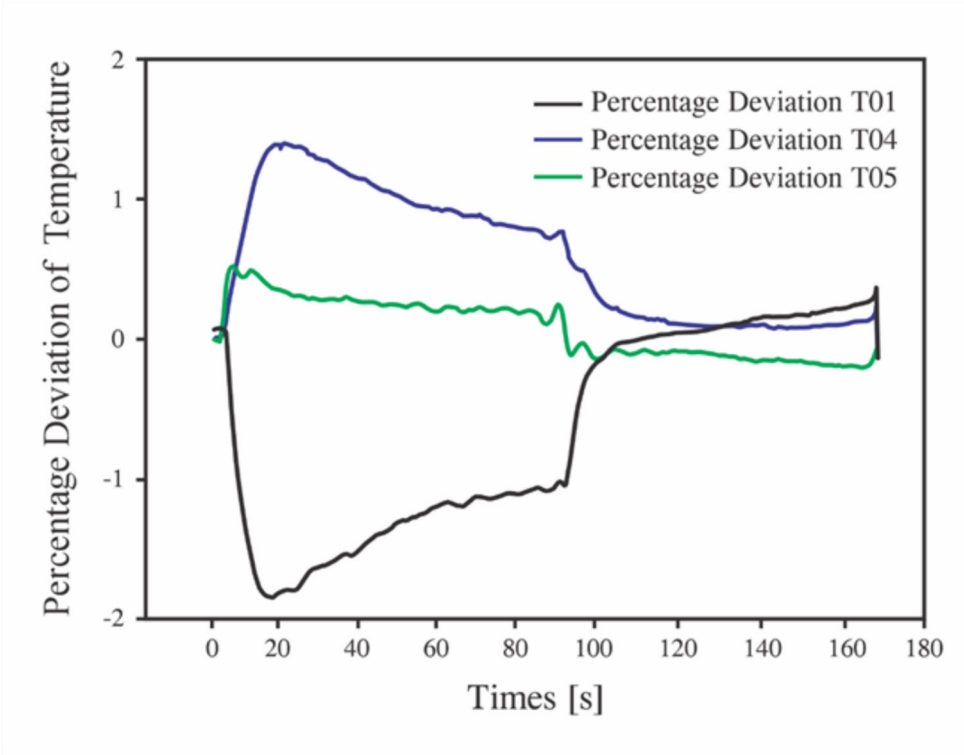

Fig. 38 Comparison between the numerical temperatures obtained by Levenberg–Marquardt and the experimental temperatures from Santos et al. (2014) for Thermocouple T03, Thermocouple T04, and Thermocouple T05

- Increasing the feed rate to 0.298 mm/rev intensifies heat generation, raising the maximum temperature to approximately 537 °C.
- The more aggressive material removal due to the higher feed rate is the primary contributor to the observed increase in temperature.

Case 4 (355 RPM, Depth of Cut: 2.0 mm, Feed Rate: 0.138 mm/rev):

- A greater depth of cut (2.0 mm) leads to slightly higher temperatures, with a peak of 461.2 °C, compared to Case 2.
- This result highlights the role of the depth of cut in affecting heat dissipation through the cutting tool.

Case 5 (28 RPM, Depth of Cut: 1.0 mm, Feed Rate: 0.138 mm/rev):

- The low rotational speed significantly reduces heat generation, with maximum temperatures not exceeding 160 °C.
- This configuration results in the lowest thermal gradients, reflecting the effect of a less severe cutting condition.

3.10 Impact of cutting parameters

Rotational Speed (RPM): Higher rotational speeds exponentially increase the temperature at the tool-chip interface due to the greater relative velocity between the tool and the workpiece.

Depth of Cut: Larger depths of cut increased the contact area, contributing to higher heat generation, though the effect is less pronounced compared to rotational speed.

Feed Rate: A higher feed rate intensifies material removal, generating more heat and raising tool temperatures. At higher feed rates, heat generation increases due to greater plastic deformation and friction at the chip-tool interface. The higher material removal rate results in intensified shearing, increasing strain rates, and converting more mechanical energy into heat. Additionally, the thicker chip leads to a larger contact area with the tool, amplifying friction and cutting forces, which further raise temperatures. In the cases studied, increasing the feed rate from 0.138 to 0.298 mm/rev (Case 3) led to a significant temperature rise to 537 °C, confirming this effect. In addition, the reduced time for heat dissipation limits the cooling effect of conduction and convection, causing heat to accumulate more rapidly. These factors demonstrate the direct relationship between feed rate and thermal effects, emphasizing the need for parameter optimization to manage excessive heat and its impact on tool wear and workpiece quality.

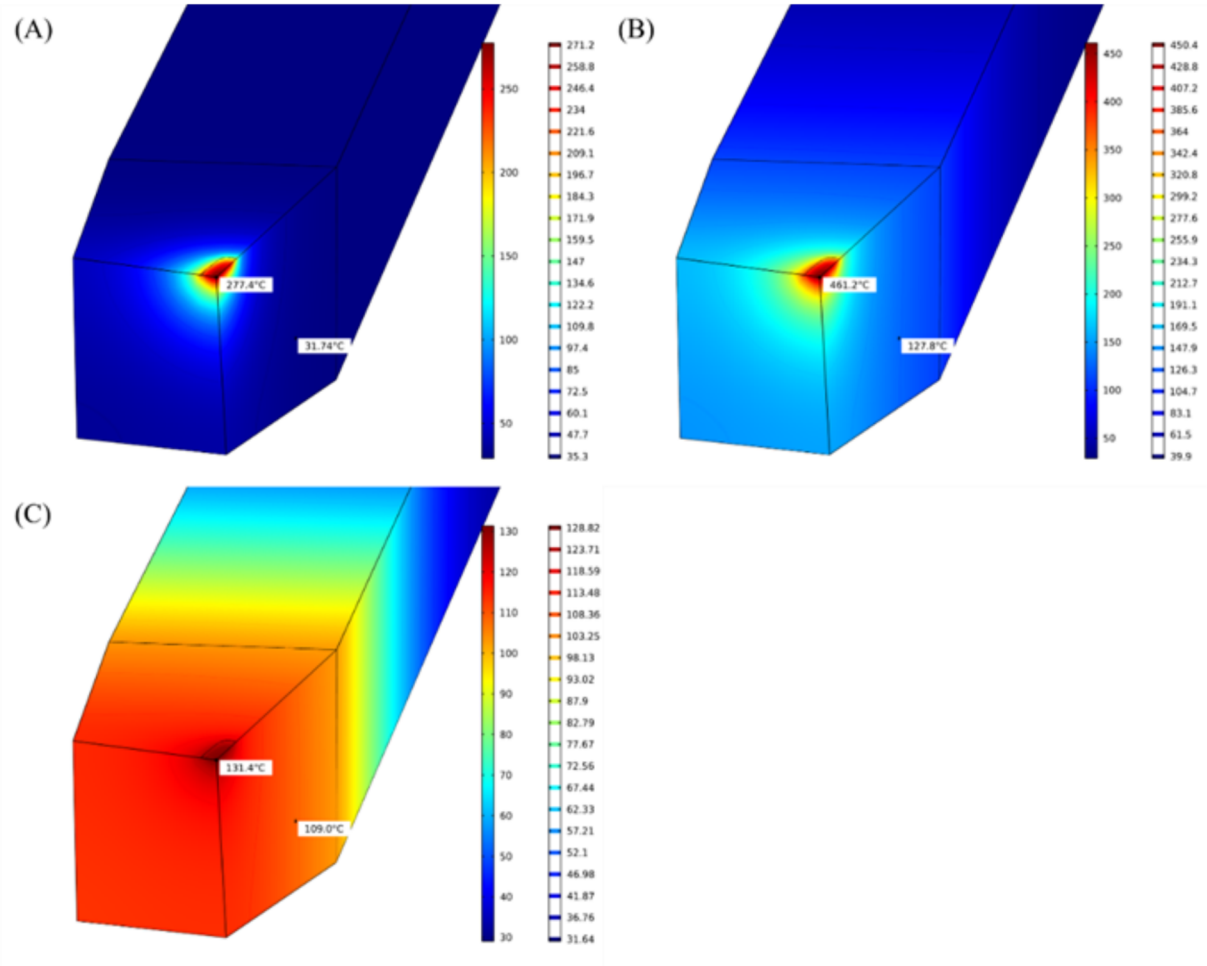

Fig. 39 Temperature field on the cutting tool for Case 4: **a** t = 5 s; **b** t = 90 s; **c** t = 110 s

The findings demonstrate that rotational speed has the most pronounced influence on tool temperature, followed by feed rate and depth of cut. To minimize tool heating and extend tool life, careful balancing of these parameters is essential, considering both process objectives and material limitations.

3.11 Thermal analysis and optimization in turning processes

The computational simulation program employed considers the convection boundary conditions obtained from the empirical formulas proposed by Incropera et al. (Kolda et al. 2003). Other available computational resources enable the definition of a material with the thermophysical properties of the cutting tool that are temperature dependent. These conditions are utilized in the comparison for convergence with the experimental results obtained by Santos et al. (2014).

Experimental protocols are meticulously devised in this investigation to mitigate potential sources of inaccuracies. The methodology described aims to determine the temperature field on the cutting tool during the machining process. Several distinctive features of this work are highlighted, such as the ability to model, in three dimensions, the thermal flow behavior and the contact area between the workpiece and the high-speed steel cutting tool as realistically as possible, using commercial computer tools. The use of a nonlinear inverse problem technique allowed for the consideration of temperature-dependent thermal properties and the effect of forced convection on the cutting tool temperature field is considered regarding standard conditions described in the experimental test developed by Santos et al. (2014).

To validate the proposed methodology, the temperature and heat flux data from the controlled experiment conducted by Carvalho et al. (2006) are considered and applied in the commercial software COMSOL® to validate the available optimization techniques through the solution of the direct heat transfer problem.

Regarding numerical analysis, initially, a 3D CAD study is developed to represent the entire cutting tool. In the present

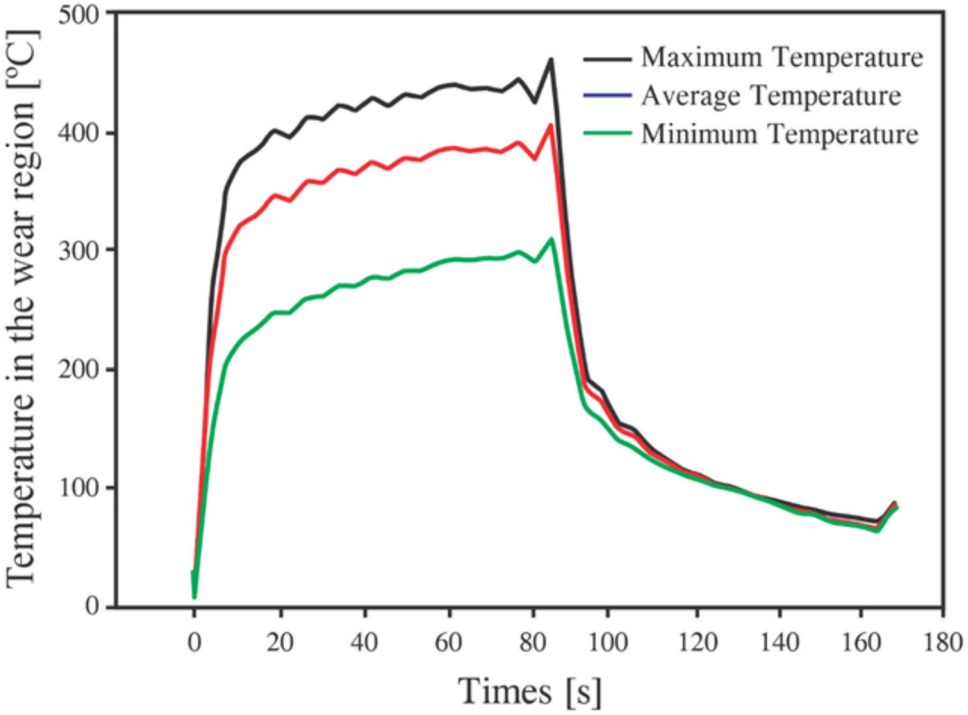

Fig. 40 Maximum, average, and minimum temperatures in the wear region for case 4

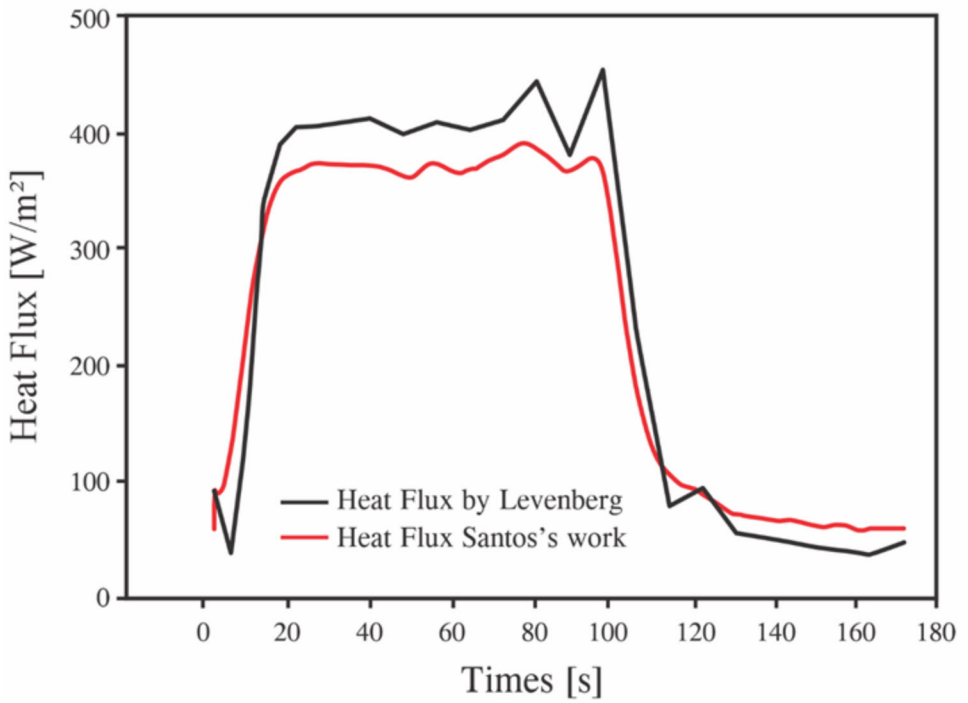

Fig. 41 Comparison between the heat flux estimated by Levenberg and the flux estimated by Santos et al. (2014) for Case 5

study, three inverse numerical techniques are employed for the estimation of numerical temperatures. Among the three techniques utilized, the one that demonstrated superior cost-effectiveness is the Levenberg–Marquardt (LM) method. The solution to the problem illustrates the efficacy of the Levenberg–Marquardt (LM) method of addressing the proposed inverse problem. The numerically estimated temperatures show a deviation of around 1.5% compared to experimental measurements when using the Levenberg–Marquardt inverse numerical technique.

Concerning the thermal effects under analysis, a comprehensive study is conducted to compute and evaluate the three-dimensional temperature distribution within the thermal machining model, including the chip-tool interface.

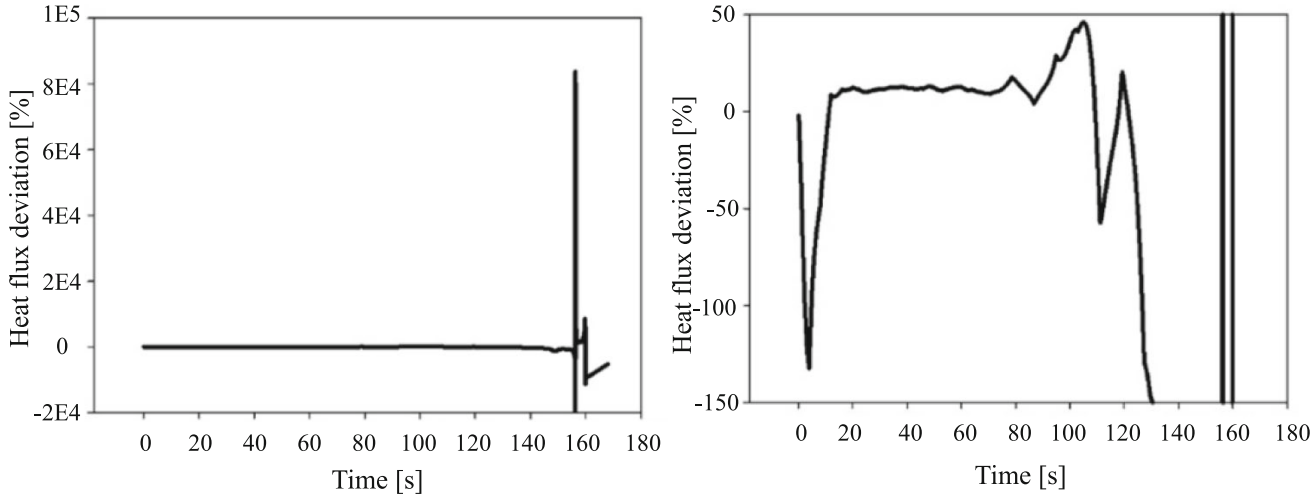

Fig. 42 Percentage deviations of heat flux; **a** overall view of the curve throughout the test; **b** zoomed-in curve emphasizing the cutting period

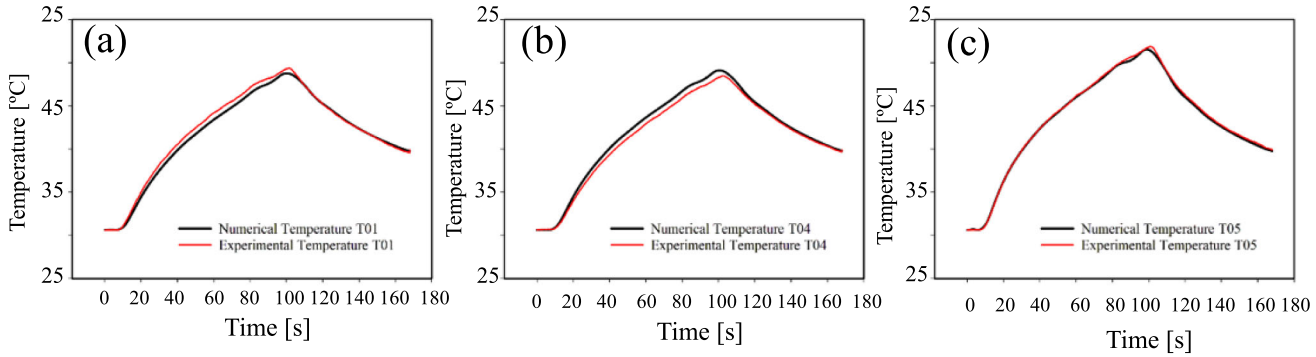

Fig. 43 Comparison of numerical and experimental temperatures; **a** Thermocouple T01; **b** Thermocouple T04; **c** Thermocouple T05

Fig. 44 Percentage temperature deviations for case 5

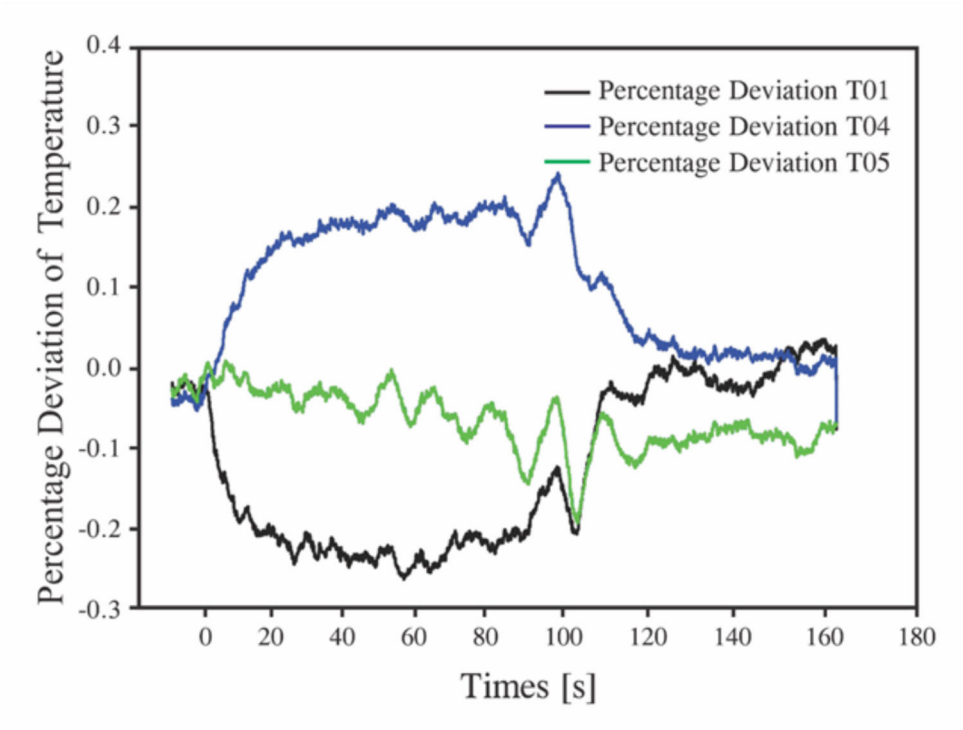

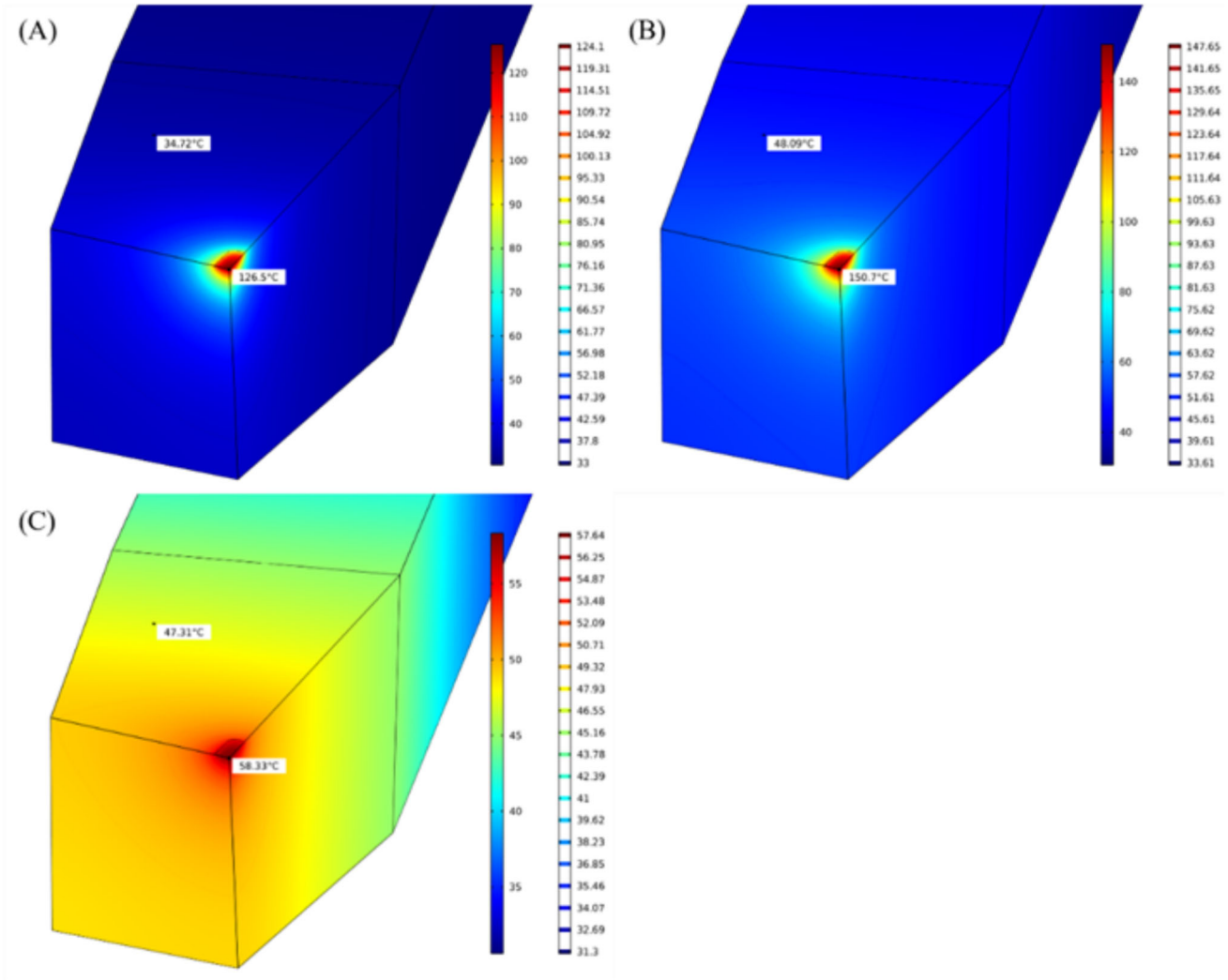

Fig. 45 Temperature field on the cutting tool for Case 5: **a** t = 20 s; **b** t = 90 s; **c** t = 110 s

Comparison of numerically derived temperatures with experimental data, provided by the experiment conducted by Santos et al. (2014), enhances the reliability and trustworthiness of the findings. Additionally, the estimation of heat flux at the contact interface facilitates quantitative analysis of thermal energy generated during the machining process.

Based on the results and given the close alignment and low percentage deviations observed in the comparisons between the numerical results obtained using the Levenberg–Marquardt optimization technique and the experimental data provided by Santos et al. (2014), it is concluded that COMSOL® Multiphysics effectively reflects the temperatures and heat flux generated in a cutting tool during a real machining process. This indicates that the methodology can be applied to adjust the cutting parameters in turning processes to achieve optimal temperature levels without compromising tool life. This approach contributes to the development and advancement of the turning process, enhancing its efficiency over time.

Analysis of the results indicates a consistent trend observed in the referenced literature, where temperatures at the cutting interface rise with increasing cutting conditions intensity. Nevertheless, deviations from findings presented by Luiz and Machado (Lewis et al. 2007), utilizing the experimental tool-workpiece thermocouple technique, are noted. Such discrepancies are attributed to inherent differences in methodologies, each carrying potential sources of error that directly influence results. Consequently, there is no universally accepted standard technique. Efforts to comprehend the fundamentals of thermal exchanges during turning operations imply a crucial step toward predicting manufacturing process performance (Nelder and Mead 1965b).

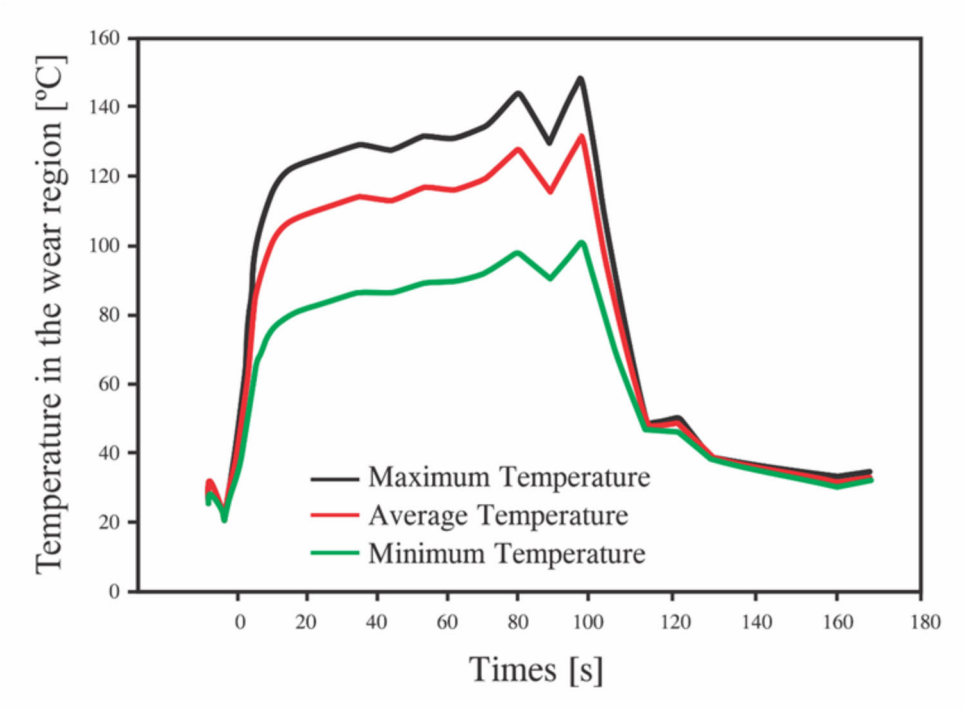

Fig. 46 Maximum, average, and minimum temperatures for Case 5

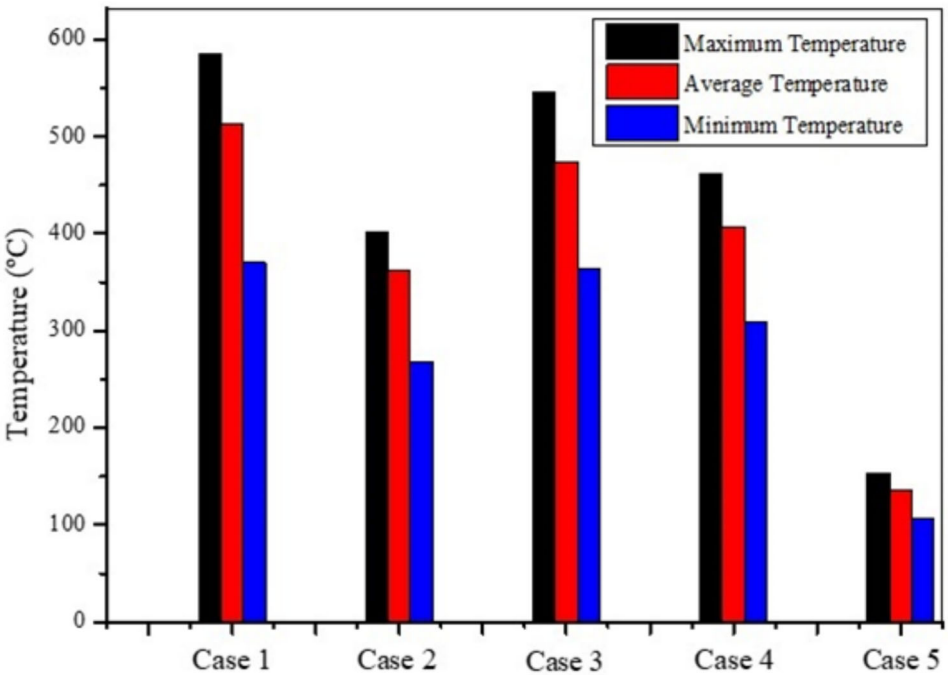

Fig. 47 Maximum, average, and minimum temperatures for Case

4 Conclusions

This study systematically investigated the influence of cutting parameters-rotational speed, depth of cut, and feed rate on the temperature distribution of an AISI M32C high-speed steel cutting tool during the machining of ABNT 12L14 steel. The results demonstrated that rotational speed was the most significant factor affecting tool temperature, followed by feed rate and depth of cut. The highest temperature (exceeding 570 °C) was observed at 900 RPM (Case 1), whereas the lowest temperature (below 160 °C) was recorded at 28 RPM (Case 5). The Levenberg–Marquardt inverse heat conduction

technique proved to be the most efficient method for estimating heat flux at the chip-tool interface, achieving deviations of less than 1.5% contrasted with experimental data.

The findings confirmed that optimizing cutting parameters was essential for minimizing tool temperature, enhancing tool life, and improving machining efficiency. The developed finite element thermal model, validated with experimental data, provided a robust framework for predictive temperature estimation in machining. Furthermore, the mesh convergence analysis ensured an optimal balance between computational efficiency and accuracy. A mesh with 6952 finite elements was selected as the most suitable configuration.

Based on the findings of this study, the optimal cutting parameters to minimize tool temperature while maintaining machining efficiency were a rotational speed between 355 and 500 RPM, a depth of cut ranging from 1.0 to 1.5 mm, and a feed rate between 0.138 and 0.200 mm/rev. A speed of 900 RPM led to excessive heat generation exceeding 570 °C, increasing tool wear, while 28 RPM significantly reduced heat transfer, without compromising machining efficiency. Similarly, increasing the depth of cut from 1.0 to 2.0 mm resulted in a temperature rise of 61 °C, highlighting the need of balancing material removal and thermal effects. Furthermore, a higher feed rate of 0.298 mm/rev caused temperatures to reach 537 °C, reinforcing that moderate feed rates offered a better trade-off between productivity and heat management. Implementing these optimized parameters could extend tool lifetime, reduce wear, and enhance machining efficiency in industrial applications. Complementary research should explore adaptive control strategies for real-time parameter adjustments based on thermal feedback. In addition to this, subsequent studies should investigate advanced cooling techniques to further improve thermal management in machining operations.

Future works should explore adaptive cooling strategies to further mitigate tool temperatures and improve tool wear resistance. Additionally, integrating machine learning algorithms with inverse heat conduction models could enhance real-time thermal predictions. This would enable smart machining systems with self-adjusting cutting parameters based on thermal feedback. Investigations into different tool coatings and materials could also provide insights into heat dissipation mechanisms, contributing to the development of more thermally resistant cutting tools.

These findings brought about practical implications for industrial machining, where controlling thermal loads is critical to ensure product quality and operational efficiency. The methodologies proposed here could be directly applied to optimize manufacturing processes, reduce tool wear, and improve energy efficiency in machining operations.

Acknowledgements The Minas Gerais State Research Foundation (FAPEMIG) supported the work, Process No. APQ-02317-18—Reg.: 42/2019, titled "Application of Inverse Problem Techniques for the Thermal Study of Machining Tools with Different Geometries and Coatings".

Author Contribution All authors contributed to the study conception and design. Material preparation, data collection, and analysis were performed by Rogério Fernandes Brito, Ricardo Luiz Perez Teixeira, Heitor Alves Falqueto, Giovani Wilhan Viana Carvalho, José Carlos de Lacerda, Tarcísio Gonçalves de Brito, Paulo Mohallem Guimarães, Sandro Metrevelle Marcondes de Lima e Silva, Solidônio Rodrigues de Carvalho, and Júlio Cesar Costa Campos. The first draft of the manuscript was written by Rogério Fernandes Brito, Ricardo Luiz Perez Teixeira, Heitor Alves Falqueto, and Giovani Wilhan Viana Carvalho and all authors commented on previous versions of the manuscript. All authors read and approved the final manuscript.

Funding This research was funded by the Minas Gerais State Research Foundation (FAPEMIG), Process No. APQ-02317-18—Reg.: 42/2019.

Data availability No datasets were generated or analysed during the current study.

Declarations

Conflict of interest The authors declare no competing interests.

References

Beck JV, Blackwell B, St. Clair C (1985) Inverse heat conduction: ill-posed problems. Wiley-Interscience Publication: New York. https://books.google.com/books?hl=pt-BR&lr=&id=-1hzLAb_ZL0C&oi=fnd&pg=PR15&ots=i0bwFQi_-e&sig=r28QePs1dcrSp7XcCq4CxTIv3gQ

Bergman TL, Lavine AS, Incropera FP, DeWitt DP (2020) Fundamentals of heat and mass transfer. 8ª edn, NJ: Ed. John Wiley & Sons, Hoboken. https://www.wiley.com/en-us/Fundamentals+of+Heat+and+Mass+Transfer%2C+8th+Edition-p-9781119353881

Bergou EH, Diouane Y, Kungurtsev V (2020) Convergence and complexity analysis of a Levenberg-Marquardt algorithm for inverse problems. J Optim Theory Appl 185(3):927–944. https://doi.org/10.1007/s10957-020-01666-1

Brito RF, Carvalho SR, Ferreira JR (2009) Thermal analysis in coated cutting tools. Int Commun Heat Mass Transfer 36(4):314–321. https://doi.org/10.1016/j.icheatmasstransfer.2009.01.009

Brito RF, Carvalho SR, Lima e Silva SMM (2015) Experimental investigation of thermal aspects in a cutting tool using COMSOL and inverse problem. Appl Therm Eng 86:60–68. https://doi.org/10.1016/j.applthermaleng.2015.03.083

Carvalho SR, Lima e Silva SMM, Machado AR, Guimarães G (2006) Temperature determination at the chip-tool interface using an inverse thermal model considering the tool and tool holder. J Mater Process Technol 179:97–104

Chen L, Tai BL, Chaudhari RG, Song X, Shih AJ (2017) Machined surface temperature in hard turning, 121:10-21. https://doi.org/10.1016/j.ijmachtools.2017.03.003

Clavier F, Valiorgue F, Courbon C, Rech J, Van Robaeys A, Mascitonio U, Brosse A, Dorlin T (2021) Numerical analysis of the tribological and geometrical impacts of tool wear on the thermo-mechanical loadings induced by 15–5PH steel turning. Proc CIRP 102:411–416. https://doi.org/10.1016/j.procir.2021.09.070

COMSOL (2018) Heat transfer module user's guide. https://doc.comsol.com/5.4/doc/com.comsol.help.heat/HeatTransferModuleUsersGuide.pdf

D'Addona DM, Raykar SJ (2019) Thermal modeling of tool temperature distribution during high-pressure coolant assisted turning. Materials 12:408. https://doi.org/10.3390/ma12030408

Diniz A, Marcondes F, Coppini N (2005) Technology of material machining. 8th. ed. Artliber: São Paulo. http://repositorio.unicamp.br/acervo/detalhe/968689

Dourado da Silva RG, Ferreira DC, Avelar Dutra FV, Lima e Silva SMM (2021) Simultaneous real-time estimation of heat flux and hot spot temperature in machining process using infrared camera. Case Stud Therm Eng 28:101352. https://doi.org/10.1016/j.csite.2021.101352

Erturk AS, Malakizadi A, Larsson R (2023) Towards an accurate estimation of heat flux distribution in metal cutting by machine learning. Procedia CIRP 117:359–364. https://doi.org/10.1016/j.procir.2023.03.061

Fernández-Abia AI, Barreiro J, Lacalle LLD, Martinez S (2011) Effect of very high cutting speeds on shearing, cutting forces, and roughness in dry turning of austenitic stainless steels. Int J Adv Manuf Technol 57:61–71. https://doi.org/10.1007/s00170-011-3267-9

Golsorkhi NA, Tehrani HA (2014) Levenberg-Marquardt method for solving the inverse heat transfer problems. J Math Comput Sci 13:300–310

Grzesik W (2017) Advanced machining processes of metallic materials: theory, modelling and applications, Ed. Elsevier Science, Oxford. https://www.sciencedirect.com/book/9780444637116/advanced-machining-processes-of-metallic-materials

Hanke M (1997) A regularizing Levenberg - Marquardt scheme, with applications to inverse groundwater filtration problems. Inverse Prob 13:79. https://doi.org/10.1088/0266-5611/13/1/007

Kanellos P, Karkalos NE, Markopoulos AP (2019) Numerical simulation of machining using a coupled FEM-CFD approach. Procedia Manuf 41:795–802

Kashani MM, Movahhedy MR, Ahmadian MT, Razavi RS (2016) Analytical prediction of the temperature field in laser-assisted machining. Procedia CIRP 46:575–578. https://doi.org/10.1016/j.procir.2016.04.071

Kolda TG, Lewis RM, Torczon V (2003) Optimization by direct search: new perspectives on some classical and modern methods. SIAM Rev 45(3):385–482. https://doi.org/10.1137/S003614450242889

Kovac P, Gostimirovic M, Rodic D, Savkovic B (2019) Using the temperature method for the prediction of tool life in sustainable production. Measurement 133:320–327. https://doi.org/10.1016/j.measurement.2018.09.074

Kshetri R, Kaushik S, Sati V, Panwar K, Ajay (2020) An investigation of cutting parameters and its effects on surface roughness in high-speed turning of 52100 bearing steel. In Advances in Materials Engineering and Manufacturing Processes: Select Proceedings of ICFTMM 2019; Springer Singapore; 105–115. https://doi.org/10.1007/978-981-15-4331-9_9

Lawson CL, Hanson RJ (1974) Solving least squares problems. Soc Ind Appl Math (SIAM). https://doi.org/10.1137/1.9781611971217

Levenberg K (1944a) A method for the solution of certain non-linear problems in least squares. Q Appl Math 2(2):164–168. https://doi.org/10.1090/qam/10666

Levenberg K (1944b) A method for the solution of certain non-linear problems in least squares. Quart Appl Math 2:164–168

Lewis RM, Shepherd A, Torczon V (2007) Implementing generating set search methods for linearly constrained minimization. SIAM J Sci Comput 29(6):2507–2530. https://doi.org/10.1137/050635432

Lian Y, Chen X, Zhang T, Liu C, Lin L, Lin F, Li Y, Chen Y, Zhang M, Zhou W (2023) Temperature measurement performance of thin-film thermocouple cutting tool in turning titanium alloy. Ceram Int 49:2250–2261. https://doi.org/10.1016/j.ceramint.2022.09.193

Lima F, Machado A, Guimarães G, Guths S (2000) Numerical and experimental simulation for heat flux and cutting temperature estimation using three-dimensional inverse conduction technique. Inverse Probl Eng 8:553–577

Lima e Silva SMM, Brito RF, Carvalho SR (2015) Experimental investigation of thermal aspects in a cutting tool using COMSOL and inverse problem. Appl Therm Eng 85:60–68. https://doi.org/10.1016/j.applthermaleng.2015.03.083

Luiz NE, Machado AR (2008) Development trends and review of free-machining steels. Proc Inst Mech Eng Part B 222(2):347–360. https://doi.org/10.1243/09544054JEM861

Machado ÁR, Coelho RT, Abrão AM, Silva MB (2015) Teoria da usinagem dos materiais. Editora Blucher: São Paulo. https://books.google.com/books?hl=pt-BR&lr=&id=9na1DwAAQBAJ&oi=fnd&pg=PA9&ots=hjLc-yZmKI&sig=aHMKTNVBYFx9L0qRZDmT7rlBpKA

Marquardt DW (1962) An algorithm for least squares estimation of nonlinear parameters. J Soc Ind Appl Math 11:431–441

Marquardt DW (1963) An algorithm for least-squares estimation of nonlinear parameters. J Soc Ind Appl Math 11(2):431–441. https://doi.org/10.1137/0111030

Marshall P (1984) Austenitic stainless steels: microstructure and mechanical properties. Elsevier, London. https://books.google.com/books?hl=pt-BR&lr=&id=hhXWZjBclvUC&oi=fnd&pg=PR5&ots=upE0ksXYae&sig=Cpe9BcAIDyZscW5Luz3K071wYwc

MATLAB (2023) Evaluate heat flux of thermal solution at nodal or arbitrary spatial locations. https://www.mathworks.com/help/pde/ug/pde.steadystatethermalresults.evaluateheatflux.html

McKinnon KIM (1999) Convergence of the Nelder-Mead simplex method to a non-stationary point. SIAM J Optimiz 9:148–158. https://doi.org/10.1137/S1052623496303482

Nelder JA, Mead R (1965a) A simplex method for function minimization. Comput J 7(4):308–313. https://doi.org/10.1093/comjnl/7.4.308

Nelder JA, Mead R (1965b) A simplex method for function minimization. Comput J 7(4):308–313. https://doi.org/10.1093/comjnl/7.4.308

Nosko O (2024) An inverse algorithm for contact heat conduction problems with an interfacial heat source based on a first-order thermocouple model. Int Commun Heat Mass Transf 158:107889. https://doi.org/10.1016/j.icheatmasstransfer.2024.107889

Oliveira AVS, Avrit A, Gradeck M (2022) Thermocouple response time estimation and temperature signal correction for an accurate heat flux calculation in inverse heat conduction problems. Int J Heat Mass Transf 185:122398. https://doi.org/10.1016/j.ijheatmasstransfer.2021.122398

PARDISO-PROJECT, 2019. https://www.pardiso-project.org. 55

Paula MA, Ribeiro MV, Souza JVC, Kondo MY (2019) Analysis of the performance of coated carbide cutting tools in the machining of martensitic stainless steel AISI 410 in dry and MQL conditions. Mater Res Express 6(29):41

Powell MJD (1973) On search directions for minimization algorithms. Math Program 4:193–201. https://doi.org/10.1007/bf01584660.S2CID45909653

Santos MR (2008) Development of a thermal model for solving inverse problems in heat transfer with application to machining of free-cutting steel using high-speed steel tools (master's thesis). Federal University of Uberlândia, Uberlândia, MG, Brazil

Santos MR, Lima e Silva SMM, Machado AR, Silva MB, Guimarães G, Carvalho SR (2014) Analyses of effects of cutting parameters on cutting edge temperature using inverse heat conduction technique. Math Prob Eng. https://doi.org/10.1155/2014/871859

Soler D, Aristimuño PX, Saez-de-Buruaga M, Garay A, Arrazola PJ (2018) New calibration method to measure rake face temperature of the tool during dry orthogonal cutting using thermography. Appl

Therm Eng 137:74–82. https://doi.org/10.1016/j.applthermaleng.2018.03.056

Spendley W, Hext GR, Himsworth FR (1962) Sequential application of simplex designs in optimization and evolutionary operation. Technometrics 4(4):441–461. https://doi.org/10.1080/00401706.1962.10490033

Teixeira RLP, de Lacerda JC, Florencio KC, da Silva SN, Henriques AB (2023) TRIP effect produced by cold rolling of austenitic stainless steel AISI 316L. J Mater Sci 58(7):3334–3345. https://doi.org/10.1007/s10853-023-08235-7

TEMPCO (2025) Kapton® Heater. https://www.tempco.com/Products/Electric-Heaters-and-Elements/Flexible-Heaters/Kapton-Heaters.htm

Thornton EA, Wieting AR (1979) Finite element methodology for transient conduction/forced-convection thermal analysis. https://doi.org/10.2514/6.1979-1100

Trent EM, Wright PK, Dearnley PA (2025) Metal cutting: theory, selection, and design. 5ª ed. Elsevier, Oxford. https://shop.elsevier.com/books/metal-cutting/trent/978-0-323-99155-1

Viale D, Béguinot J, Chenou F, Baron G (2002) Optimizing microstructure for high toughness cold-work tool steels. In: Proceedings of the 6th International Tooling Conference, September 2002, 299–318. https://www5.kau.se/sites/default/files/Dokument/subpage/2010/02/23_299_318_pdf_14207.pdf

Yu WC (1979a) Positive basis and a class of direct search techniques. Sci Sinica 1(26):53–68

Yu WC (1979b) The convergent property of the simplex evolutionary technique. Sci Sinica 1:68–77

Zhenwu F, Han B, Chen Y (2022) Levenberg-Marquardt method with general convex penalty for nonlinear inverse problems. J Comput Appl Math 404:113771. https://doi.org/10.1016/j.cam.2021.113771. (**ISSN 0377-0427**)